Isomeric and hybrid ferrocenyl/cyrhetrenyl aldimines: a new family of multifunctional Compounds†

Juan Oyarzo, [a] Alejandra Acuña, [a] Hugo Klahn, [*a] Rodrigo Arancibia, [b]
Carlos P. Silva, [c] Ramón Bosque, [d] Concepción López, [*d]
Mercè Font-Bardía, [e] Carme Calvis [f] and Ramón Messeguer [f]

a Instituto de Química, Pontificia Universidad Católica de Valparaíso, Casilla 4059, Valparaíso, Chile.
b Laboratorio de Química Inorgánica y Organometálica, Departamento de Química Analítica e Inorgánica, Facultad de Ciencias Químicas, Universidad de Concepción, Concepción, Chile
c Departamento de Química de los Materiales, Facultad de Química y Biología, Universidad de Santiago de Chile, Casilla 40, Correo 33, Santiago, Chile; Soft Matter Research and Technology Center, SMAT-C, Santiago, Chile
d Department de Química Inorgànica i Orgànica (Secció de Química Inorgànica), Facultat de Química, Universitat de Barcelona, Martí i Franquès 1–11, 08028-Barcelona, Spain. e Unitat de Difracció de Raigs-X, Centre Científics i Tecnològics (CCiT), Universitat de Barcelona, Solé i Sabaris 1–3, 08028 Barcelona, Spain
f Biomed Division, LEITAT Technological Centre, Parc Científic de Barcelona,Edifici Hèlix, Baldiri i Reixach 13-21, 08028-Barcelona, Spain

Hugo Klahn: hugo.klahn@pucv.cl
Concepción, Chile: conchi.lopez@qi.ub.es

ABSTRACT:

The synthesis and characterization of two novel and isomeric hybrid ferrocenyl/cyrhetrenyl aldimines [(η5-C5H5)Fe{(η5-C5H4)-CHvN-(η5-C5H4)}Re(CO)3] (1) and [(η5-C5H5)Fe{(η5-C5H4)-NvCH-(η5-C5H4)}Re (CO)3] (2) are reported. Their X-ray crystal structures reveal that both adopt the E form. However, molecules of 1 and 2 differ in the relative arrangement of the "Fe(η5-C5H5)" and "Re(CO)3" units (anti in 1 and syn in 2). This affects the type of intermolecular interactions, the assembly of the molecules and therefore their crystal architecture. Comparative studies of their electrochemical, spectroscopic and photo-physical properties have allowed us to clarify the effect produced by the location of the organometallic arrays (ferrocenyl or cyrhetrenyl) on electronic delocalization, the proclivity of the metals to undergo oxidation and their emissive properties. Theoretical studies based on Density Functional Theory (DFT) calculations on the two compounds have also been carried out in order to rationalize the experimental results and to assign the bands detected in their electronic spectra. The cytotoxic activities of compounds 1 and 2 against human adenocarcinoma cell lines [breast (MCF7 and MDA-MB-231) and colon (HCT-116)] reveal that imine 2 has a greater inhibitory growth effect than 1 and it is ca. 1.8 times more potent than cisplatin in the triple negative MDA-MB 231 and in the cisplatin resistant HCT-116 cell lines. A comparative study of their effect on the normal and non-tumour human skin fibroblast BJ cell lines is also reported.

INTRODUCTION

Heterodimetallic compounds have attracted great interest in recent years. The presence of two proximal metals with different environments, oxidation numbers and spin states may influence their mutual cooperation, reactivity, electrochemical behaviour, photo-optical properties and also activities (i.e. catalytic, biological).1–4 Besides this, the proper selection of two metal ions, their environments and their connectivity (i.e. by metal–metal bonds, ligands' scaffold or functional groups) may also produce multifunctional compounds with outstanding relevance in new materials design (i.e. electrochemical devices, sensors, molecular switches, etc.), photoelectronic technology, nanoscience, catalysis, biology and medicine.5

On the other hand, bioorganometallic chemistry has been one of the research areas with a greater, and also faster, development during the last decade.6,7 The great advances achieved so far as well as the discovery of relevant applications of organometallic compounds in diagnosis, therapy and imaging are promoting the interest of a large number of scientists, making this area more attractive day after day. Among the huge variety of organometallic compounds, metallocenes (especially ferrocene derivatives) and three-legged half sandwich organometallic derivatives are the most promising candidates in biotechnology, diagnosis and new drug design. Examples of their use as bioprobes for cellular imaging, pharmaceutical sensors, molecular recognizers, detectors, and artificial metallo-enzymes have been described, and the idea of using these organometallic complexes in new drug (or prodrug) discovery is becoming more and more fascinating and popular.8–11

The success of ferrocenyl-based molecules as antimalarial, antitumoral, anti-VIH, antibacterial, and antifungal agents and inhibitors8–11 has triggered the interest on novel ferrocene derivatives with greater efficiencies, lower toxicities and minor side effects than the drugs used nowadays for the treatment of these diseases. It has also allowed the extension of the strategies used for ferrocenes to the half-sandwich organometallic compounds. Those with fac-[M(CO)3] cores, such as cyrhetrene [Re(η5-C5H5)(CO)3] and cymantrene [Mn(η5-C5H5)(CO)3] derivatives, are attracting a great deal of interest in new medicinal chemistry due to their high stability in air and water, lipophilicity, low toxicity, properties (i.e. photo-physical or electrochemical) or biological activities.11–18

Cyrhetrene chemistry has undergone a fast and spectacular growth in the last five-years.11–18 The development of new hybrid compounds with the "[Re(η5-C5H4)(CO)3]" unit anchored on the backbones of molecules of biological relevance is one of the most active and promising areas of research in new medicinal chemistry. The compounds shown in Fig. 1 are representative examples to illustrate the relevance of cyrhetrenyl derivatives in bioorganometallic chemistry. The amides and sulphonamides (A and B in Fig. 1) are capable of pharmaceutical sensors, molecular recognizers, detectors, and artificial metallo-enzymes have been described, and the idea of using these organometallic complexes in new drug (or prodrug) discovery is becoming more and more fascinating and popular.8–11

The success of ferrocenyl-based molecules as antimalarial, antitumoral, anti-VIH, antibacterial, and antifungal agents and inhibitors8–11 has triggered the interest on novel ferrocene derivatives with greater efficiencies, lower toxicities and minor side effects than the drugs used nowadays for the treatment of these diseases. It has also allowed the extension of the strategies used for ferrocenes to the half-sandwich organometallic compounds. Those with fac-[M(CO)3] cores, such as cyrhetrene [Re(η5-C5H5)(CO)3] and cymantrene [Mn(η5-C5H5)(CO)3] derivatives, are attracting a great deal of interest in new medicinal chemistry due to their high stability in air and water, lipophilicity, low toxicity, properties (i.e. photo-physical or electrochemical) or biological activities.11–18 Cyrhetrene chemistry has undergone a fast and spectacular growth in the last five-years.11–18 The development of new hybrid compounds with the "[Re(η5-C5H4)(CO)3]" unit anchored on the backbones of molecules of biological relevance is one of the most active and promising areas of research in new medicinal chemistry. The compounds shown in Fig. 1 are representative examples to illustrate the relevance of cyrhetrenyl derivatives in bioorganometallic chemistry. The amides and sulphonamides (A and B in Fig. 1) are capable of inhibiting carbonic anhydrase enzymes.11d Several families of cyrhetrene conjugates with tamoxifen, hydroxytamoxifen (Fig. 1, C)12 and chloroquine (Fig. 1, D)13 have been prepared and evaluated as antitumoral or antiparasitic agents against malaria, leishmaniasis or trypanosomiasis.13,14 Compound D has remarkable activity (IC50 = 0.9 μM) against Trypanosoma brucei and low toxicity to normal human cells. Kowalski and co-workers have recently reported seven new hybrid cyrhetrene/nucleobase derivatives, of which the uracil conjugates (Fig. 1, E) resulted to be the most active.14

Other families of cyrhetrene derivatives containing crown ethers, chalcones and azoles as pendant arms15 or incorporating functional groups of biological relevance (i.e. thiosemicarbazones, azines, imines) have also been prepared and evaluated as antiparasitic agents.16,17 Imines (Fig. 1, F) (more cytotoxic than their ferrocenyl analogues and nifurtimox) are amongst the most potent anti-Trypanosoma cruzi agents reported so far.17 These findings suggested that the assembly of the cyrhetrenyl unit and the imine group enhances their anti-Chagas activity. Besides this, the furyl derivative (Fig. 1, F) (with XvO) produces reactive oxygen species that may be relevant in view of their potential antitumoral activity.17d Despite these findings, and the ongoing interest on (a) ferrocenylimines as antitumoral drugs themselves or as ligands to achieve transition metal complexes with enhanced cytotoxic activity (representative examples are shown in Fig. 2)18,19 and (b) cyrhetrenyl derivatives with relevant photophysical properties and biological activities (or both simultaneously),12–17 mixed ferrocenyl/cyrhetrenyl imines are still unknown.

Herein, we present the two novel aldimines R1-CHvN-R2, with R1 = ferrocenyl and R2 = cyrhetrenyl (1) or vice versa (2) (Chart 1) as the first examples of small molecules containing both organometallic fragments connected by the imine functionality. Experimental work and computational studies on compounds 1 and 2 clarify the effects produced by the interchange of the two organometallic arrays on their structures, stabilities and properties (electrochemical and photo-physical). Also, their effect on two

137 breast cancer cell lines (MCF7 and triple negative MDA-MB231), the HCT116 colon cancer cell line,
138 and the non-tumoral human skin fibroblast BJ cell line has been studied.
139

RESULTS AND DISCUSSION

Synthesis and characterization of the compounds

In the first attempt to achieve the synthesis of the aldimine (1), we decided to use the procedure described previously for the ferrocenylimines [(η5-C5H5)Fe{(η5-C5H4)-CHvN-R1}] (R1 = phenyl or benzyl)20,21 that consisted of the reaction of equimolar amounts of the aldehyde [(η5-C5H5)Fe{(η5-C5H4)-CHO}] and the corresponding amine H2N-R1 in refluxing benzene (or toluene) and using Dean Stark apparatus to remove the benzene (or toluene)–water azeotrope formed. When the reaction was carried out using cyrhetrenylamine and toluene as solvents, the IR spectra as well as the results obtained from thin layer chromatography (TLC) of the solution obtained after long refluxing periods (up to two days) revealed the coexistence of small amounts of the desired aldimine (1) and ferrocenecarboxaldehyde as the major product. This problem is similar to that found for related ferrocenylimines [(η5-C5H5)Fe{(η5-C5H4)-C(R2)vN-R1}] with bulky substituents (i.e. R1 = phenyl rings and R2 = Ph or Me),21–23 which were finally obtained with the aid of activated alumina or molecular sieves to fulfil the condensation process. In view of this we decided to explore whether the presence of molecular sieves could improve the process. In this case (Scheme S1, A†), the progress of the reaction was monitored by IR and TLC and after 24 h, both revealed the absence of the aldehyde. The 1H-NMR spectrum of the solid obtained after concentration confirmed the formation of imine 1. This compound was finally purified by diffusion at −18 °C of a CH2Cl2 solution of the raw material layered with n-hexane.

The preparation of imine 2, which can be visualized as arising from 1 by a simple interchange of the ferrocenyl and cyrhetrenyl groups, was much easier than that of imine 1. This was achieved by the treatment of [(η5-C5H5)Fe{(η5-C5H4)-NH2}] and [Re{(η5-C5H4)-CHO}(CO)3] in a 1 : 1 molar ratio and in refluxing toluene (Scheme S1, B†) but using milder experimental conditions than for 1: shorter refluxing periods {12 h (for 2) versus 24 h (for 1)}, in the absence of molecular sieves and without the aid of Dean Stark apparatus.

The new aldimines were isolated in fairly good yields (80% and 85% for 1 and 2, respectively). They are air-stable solids at room temperature and exhibit high solubility in CH2Cl2, CHCl3, toluene, acetone and acetonitrile, but they are practically insoluble in hexane. As we will demonstrate later on (see below), compound 1 hydrolyses slowly in CDCl3 solution at 298 K.

Compounds 1 and 2 were characterized by mass (HRMS and EI) and infrared spectra, X-ray diffraction and NMR. Their HRMS spectra showed a peak with the expected isotopic pattern at m/z = 547.9945 (for 1) and 547.9939 (for 2) that agree with the calculated value for their [M + H]+ cations (m/z = 547.9954). The EI spectra of compounds 1 and 2 showed the peaks of the molecular ions and the fragments formed by the successive loss of the CO ligands.

The common features observed in the IR spectra of 1 and 2 (Experimental section) are (a) the existence of the typical intense bands of the cyrhetrenyl units in the range of 2020–1930 cm−1 that are ascribed to the stretching of the pendant CO groups and (b) the presence of another and less intense band at ca. 1615 cm−1. The position of this band is similar to the values reported for ferrocenyl20,21 and cyrhetrenyl aldimines17 and is assigned to the stretching of the >CvN– functional group.

It is well known that (a) imines may adopt two different forms (E or Z) in solution as well as in the solid state23 and (b) the presence of bulky substituents attached to the atoms of the >CvN– group may hinder the free rotation around the C–R1 and or N–R2 bonds giving rotameric species.24,25 In aldimines 1 and 2, the two substituents (ferrocenyl and cyrhetrenyl) are bulky and therefore, two different arrangements of the "Fe(η5-C5H5)" and "Re(CO)3" units could be expected for the (E) and (Z) forms of the imine. This is especially relevant in the solid state, because it affects not only the Fe···Re separation but also the arrangement of the rings, which could introduce significant changes on the assembly of the units in the crystal and the crystal architecture.

Fig. S1† shows a set of isomers (a–d) for compound 1. In the pair (a, b), the imine has the E form, while in c and d it adopts the Z form. The two isomers of each pair {(a, c) and (b, d)} differ in the relative disposition of the two metal ions (Fe and Re) in relation to the main plane (herein after referred to as MP and defined by the two substituted "C5H4" rings and the connector (>CvN– group)). The two metal ions may be located on the opposite sides of the MP plane {anti (in a and c)} or in the same side {syn (in b and d)}. Although this is not shown in Fig. S1,† a similar set of isomeric forms could also be expected for imine 2.

Good X-ray quality red monocrystals of [(η5-C5H5)Fe{(η5-C5H4)-CHvN-(η5-C5H4)}Re(CO)3] (1) and [(η5-C5H5)Fe{(η5-C5H4)-NvCH(η5-C5H4)}Re(CO)3] (2) were obtained by slow evaporation at −18 °C of their CH2Cl2 solutions layered with n-hexane.

Description of the crystal structures of the new aldimines (1 and 2)

The crystal structures of compounds 1 and 2 (Fig. 3 and 4, respectively) confirmed the presence of the two organometallic units (ferrocenyl and cyrhetrenyl) connected by the functional >CvN– group. A selection of bond lengths, bond angles and relevant angles between planes is presented in Table 1. Bond lengths and angles of the ferrocenyl unit fall in the range expected for related ferrocenylaldimines;20,21,26 the pentagonal rings are planar, and nearly parallel [tilt angles = 1.3° (in 1) and 1.1° (in 2) and they deviate by ca. 3.7° and 5.3° (in 1 and 2, respectively) from the ideal eclipsed conformation. In both cases, (a) Re(I) exhibits the typical three legged piano stool geometry bound to three CO ligands and the substituted C5H4 ring in a η5 fashion and (b) bond distances and angles of the cyrhetrenyl unit are similar to those found in monosubstituted [Re(η5-C5H4R)(CO)3] compounds.17,26,27

The >CvN– bond length in compounds 1 and 2 is identical [C11–N1: 1.276(6) Å]. For 1 this value is similar to that of [(η5-C5H5)Fe{(η5-C5H4)-CHvN-R1}] (R1 = substituted phenyl rings),25,26 while in

2 this is clearly greater than that found in [Re{(η5-C5H4)-NvCHR4}(CO)3] with R4 = 4-nitrofuryl [1.266(15) Å].17c

As shown in Fig. 3 and 4, the organometallic arrays are in a trans-disposition [torsion angles: C12–N1–C11–C10: 175.9(4)° (in 1) and C10–N1–C11–C12: 179.72(16)° (in 2)] confirming that both aldimines adopt the E form in the crystals. However, the relative arrangement of "Re(CO)3" and "Fe(η5-C5H5)" is markedly different: anti in 1 and syn in 2. On these bases, the crystal structure of compound 1 corresponds to isomer a (Fig. S1†), but that of aldimine 2 matches isomer b (Fig. S1†). As a consequence of this, the distance Fe⋯Re in 1 (7.114 Å) is bigger than that in 2 (6.122 Å) and both clearly exceed the sum of their van der Waals radii [Fe: 2.19 Å and Re 2.35 Å].28 Moreover, in 1, the two C5H4 rings are less coplanar than in 2 (angle between their main planes are 12.6° and 7.7°, respectively). This is also relevant because it is well-known that deviations from co-planarity between aromatic rings are commonly associated with a decreese of electronic delocalization.

The different arrangement of the "Fe(η5-C5H5)" and "Re(CO)3" units in compounds 1 and 2 also affects the assembly of the molecules in the crystals. In compound 1, a molecule sited at (x, y, z) is connected by C–H⋯π interactions involving (a) the C2–H2 bond and the ring defined by the set of atoms [C12–C16] (Fig. S2†) of another unit at (–x, y, 12 − z) and (b) the H13 atom and the C5H5 ring of the ferrocenyl group belonging to a molecule on (−x, −1 + y, 12 − z). Additional C–H⋯O short contacts between the oxygen atoms of the hanging CO ligands and the hydrogen atoms of three proximal molecules (Fig. S2†) extend the assembly of the molecules in the crystals.

In contrast with the results obtained for 1, in the crystals molecules of 2 are assembled by two co-operative π stacking interactions (Fig. S3†), involving the substituted ring of the ferrocenyl unit of a molecule and the C5H4 ring of another and proximal one with a head-to-tail orientation, and vice versa giving dimers (the distance between the centroids of the two rings being 3.498 Å). Additional intermolecular C–H⋯O interactions between (a) the O1 atom of one molecule and the C8–H8 bond (of the ferrocenyl group) of a different unit and (b) the O3 atom the C5–H5 bond of the cyrhetrenyl group of another molecule fulfil the assembly of the dimers.

Solution studies

1H and 13C-NMR data for both compounds are presented in the Experimental section. In both cases, the assignment of the signals detected in their spectra has been achieved with the aid of two-dimensional [1H–1H] NOESY and [1H–13C] HMBC NMR experiments. In the 1H-NMR spectra of the two aldimines the resonance of the iminic proton appeared as a singlet at 8.29 ppm (for 1) or 8.18 ppm (for 2). The position of these signals agrees with that reported for ferrocenylimines [(η5-C5H5)Fe{(η5-C5H4)-CHvN-R1}] (with R1 = phenyl group)20,21,25 and for the cyrhetrenyl derivatives [Re{(η5-C5H4)-CHvN-R1}],17 respectively, which adopted the E form in the solid state and also in CDCl3. This indicated that imines 1 and 2 retained the (E)-form in solution (2D-NMR studies described below confirmed this finding). At higher fields (4.0 ppm < δ < 6.0 ppm), the 1H-NMR spectra showed a set of

five signals: an intense singlet due to the protons of the C5H5 ring, and four triplets (of identical intensity) that correspond to the two types [(H2 and H5) and (H3 and H4)] of different protons of in each C5H4 unit. Additional 2D-NMR experiments ([1H–1H] NOESY and [1H–13C] HMBC) allowed us to fulfil the assignment of the signals.

The [1H–1H] NOESY spectra of freshly prepared solutions of 1 and 2 in CDCl3 at 298 K showed cross peaks between the resonances due to the imine proton at around 8.1 ppm and those of the protons on the ortho sites of the two C5H4 rings [pairs (H2 and H5) and (H2 and H5)]. This confirmed the E form of the imines 1 and 2 in solution and also the identification of the signals due to the two types of protons of each ring.

13C{1H} NMR spectra of 1 and 2 in CDCl3 at 298 K exhibited a singlet in the low field region (ca. $\delta \approx$ 193 ppm) that corresponds to CO ligands. The resonance due to the imine carbon appeared at 166.6 ppm (for 1) and at 148.9 ppm (for 2). The position of these signals is in good agreement with those reported for closely related aldimines [(η5-C5H5)Fe{(η5-C5H4)-CHvN-R1}] (R1 = phenyl group)20,21,25 and for the cyrhetrenyl derivative type F shown in Fig. 1.17 The up-field shift of the resonance due to the imine carbon observed for 2 (ca. 18 ppm) in relation to that of 1 suggests that the interchange of the ferrocenyl and cyrhetrenyl units produces a significant change in the electronic density of the >CvN– moiety. In both cases the signals due to the ipso carbon atoms of the C5H4 rings (C1 and C1) exhibited low intensity, appeared in the range 78 ppm $\leq \delta \leq$ 130 ppm and their chemical shifts were clearly affected by the nature of the atom to which they are bound (Nimine or Cimine). At higher fields a set of five additional signals were also observed, of which the most intense one corresponds to the carbon nuclei of the C5H5 ring and the remaining ones to the two pairs of carbon atoms [(C2 and C5) and (C3 and C4)] of each C5H4 ring (see characterization data for the two compounds).

Study of the stability of compounds 1 and 2 in solution. The stability of the two aldimines in solution has also been investigated by comparing the 1H-NMR spectrum of a freshly prepared solution of the corresponding compound in CDCl3, CD3CN or DMSO-d6 with those registered after different periods of storage (t) at 298 K.

The 1H-NMR spectrum of the freshly prepared solution of 1 in CDCl3 at 298 K changed with time (Fig. S4†) and after 4 h of storage additional signals with tiny intensity were also detected. For t = 18 h the changes became more evident and in this case the analyses of the resonances observed suggested the coexistence of the aldimine, ferrocenecarboxaldehyde and the amine in a relative abundance: 1.00 : 0.78 : 0.77. Thus, this indicates that compound 1 hydrolyzes slowly in CDCl3. In contrast with the results obtained for 1, no significant variations in the 1H-NMR spectrum of 2 were detected after long storage periods (up to five days) (Fig. S5†), thus indicating that 2 is more stable than 1 in CDCl3 and less prone to hydrolyze.

In order to check also the stability of the aldimines in the solvent used for the electrochemical studies (see the following section), a parallel study was carried out using acetonitrile-d3 (Fig. S6†). In this case

no significant changes in their NMR spectra were detected after several hours of storage, indicating that both compounds are stable in this solvent at 298 K.

As mentioned above compounds holding ferrocenyl arrays and organometallic transition metal complexes with pianostool geometries and fac-[M(CO)3] cores are gaining importance due to their potential biological activity and utility. In view of this and since for the biological studies described below, the first step consisted in the dissolution of the compound in DMSO, followed by subsequent dilutions with water, the stability of the new products in DMSO-d6 was also investigated by 1H-NMR. As shown in Fig. S7,† the narrow signals observed in the spectrum of the freshly prepared solution of 1 in DMSO-d6 broaden with time. After 4 h, the spectrum showed new sets of signals of which one was due to ferrocenecarboxaldehyde, probably formed by hydrolysis of the imine group. In contrast with these results 1H-NMR studies of compound 2 (Fig. S8†) revealed that it is much more stable and robust than 1 in DMSO-d6. An additional study was carried out with compound 2 using a DMSO-d6 : D2O (4 : 1) mixture showing that it remained practically unaltered under these experimental conditions (298 K) for several days. The 1H-NMR spectrum registered after 112 h of storage indicated the presence of 2 as the major product and small amounts of the degradation product (Fig. S9†).

Comparative study of their electrochemical, photo-optical and biological activities

Electrochemical behaviour. The electrochemical properties of new isomeric ferrocenyl/cyrhetrenyl aldimines 1 and 2 were also investigated. As shown above, NMR studies confirmed that both aldimines were stable in acetonitrile. The electrochemical studies were carried out by cyclic voltammetry of freshly prepared solutions (10−4 mol L−1) in acetonitrile with (Bu4N)[PF6] as the supporting electrolyte. All these experiments were carried out at a scan rate υ = 250 mV s−1. Cyclic voltammograms (hereinafter referred to as CVs) are shown in Fig. 5 and a summary of electrochemical data for compounds under study is presented in Table 2.

The CVs of the new aldimines showed in the range −1.20 V < E < 0.50 V (Fig. 5A) an oxidation peak (I) with a directly associated reduction one in the reverse scan (I′), the intensity ratio (Ipa/Ipc) was close to 1 and the separation between the oxidation and reduction peaks ΔE = (EIpa − EI′ pc was similar to that obtained for ferrocene under identical experimental conditions. These findings agree with those expected for a simple reversible one electron-process.29 It is well-known that the proclivity of ferrocene derivatives to oxidize is strongly dependent on the nature of the substituents.9,30 In general, the presence of electron withdrawing groups produces an increase of the Epa value, while donor groups have the opposite effect.

For compound 1 the position of the wave and the anodic potential are similar to those for ferrocenylaldimines of general formulae [(η5-C5H5)Fe{(η5-C5H4)-CHvN-R4}] and especially to those with R4 = CH2-C6H5 {EI pa = 0.20 V30} under identical conditions. This suggests that the effect produced by the Re(η5-C5H5)(CO)3 unit on the proclivity of Fe(II) to oxidize is similar to that of the

benzyl group. In contrast with these results, for isomer 2, the wave shifts to the more cathodic region, thus indicating that the "–NvCH(η5-C5H4)Re(CO)3" unit is a stronger electron-donor group than "–CHvN(η5-C5H4)Re(CO)3".

Besides this, the anodic potential (EI pa) of 2 is quite close to that of ferrocene itself, and therefore more prone to oxidize than 1. It is well-known that in biological systems the accessible redox potential window ranges only from around −0.40 to +0.80 V versus the normal hydrogen electrode (NHE).31 Compound 2 has a redox potential quite close to that of ferrocene [E(Fc/Fc+) = 0.5 V versus NHE] and in the range of the biological systems, while that of the aldimine 1 is higher and closer to the upper limit of the biological range. This differential behaviour may be important in view of their potential utility in drug design or for their use as biomarkers.

When the cyclic voltammograms were registered in a wider range of potentials [from −1.00 V to +1.60 V], an additional and poorly resolved oxidation peak (II in Fig. 5B) was observed. The potential of this peak [EIIpa = 1.29 V (for 1) and 1.42 V (for 2)] falls in the range reported for other cyrhetrene derivatives and has been assigned to the typical oxidation of Re(I) to Re(II).15a In the reverse scan (Fig. 5B), two (for 1) or three (for 2) additional reduction peaks were detected in the range −0.4 V < E < 0.4 V, of which one (I′) corresponds to the reduction of Fe(III) formed during oxidation.

These studies provide conclusive evidence of the effect produced by the location of the ferrocenyl and cyrhetrenyl arrays in the aldimines R1-CHvN-R2. The shifts detected in the position of anodic peaks (EIpa and EII pa) for the two isomers suggest that the interchange of the two organometallic units produces a significant variation in the electronic distribution of charge. In both cases, the first anodic peak (I) corresponds to the oxidation of the Fe(II) centre, but for 2 it occurs at lower potentials than for 1, thus suggesting that the energy level of the HOMO of 2 is higher than that of 1. Computational studies described below confirm this hypothesis.

Absorption and emission spectra. As mentioned in the Introduction section, one of the most attractive properties of compounds holding fac-[M(CO)3] units arises from their potential luminescence that may allow their use as luminescent probes or sensors. Since the new aldimines contain this array we also investigated their photophysical properties. First, the UV-vis spectra of 10−4 mol L−1 solutions of compounds 1 and 2 in CH2Cl2 at 298 K were registered (Fig. 6 and Table 3). In both cases three (for 1) and four (for 2) intense absorption bands (with extinction coefficients, ε in the range of 10−3–10−4M−1 cm−1) were observed. The position of the band at lower energies (λ ≈ 475 nm) agrees with that of related ferrocenyl imines and hydrazones32 and has been attributed to a d–d transition of the Fe(II) centre. Computational studies (see the following section) confirmed this assignment. In the UV-vis spectrum of complex 2 (Fig. 6), another absorption maximum at λ = 383 nm was observed, which is characteristic of cyrhetrene derivatives.11,32,33 For 1 this band is not observed in the spectrum probably due to the presence of more intense bands at lower wavelengths that may mask it. In both cases two additional and more intense bands were also detected in the range of 220–320 nm.

361 Due to the increasing attractiveness of luminescent Re(I) complexes with “Re(CO)3” arrays,6,8,11,12
362 we also investigated the emissive properties of the new aldimines in CH2Cl2 at 298 K. Upon excitation
363 at 477 nm, both complexes showed an emission band at 551 nm (Fig. 7A), which, according to the
364 literature, 33 originates from a 3MLCT phosphorescence state.
365 As mentioned above, the UV-vis spectrum of compound 2 showed also an additional absorption band λ
366 = 383 nm, and after excitation at 385 nm, the emission spectra of 2 (Fig. 7B) showed three bands in the
367 range 400 nm ≤ λ ≤ 500 nm. When the experiment was carried out under identical conditions, but using
368 1 instead of 2, the emission spectra showed a similar pattern (Fig. 7B). This suggests that the typical
369 band of the “Re(CO)3” unit was not observed in the UV-vis spectrum. The spectrum of 1 was probably
370 masked by the intense absorption at higher energies (λ = 314 nm). Time-dependent DFT calculations
371 (see below) confirmed this hypothesis.
372 Computational studies. As mentioned above, multifunctional compounds with potential utility in new
373 materials and technological development are attracting a great deal of inter-est due to their potential
374 utility in new materials design and technological devices.5 The new aldimines exhibit interesting
375 photophysical and electrochemical properties and in addition it is well known that imines are valuable
376 reagents in organic and organometallic synthesis.34 In view of these and in order to compare the
377 stability of the isomers of 1 and 2 and to explain the effect produced by the interchange of the two
378 organometallic arrays in R1-CHvN-R2 on their stability, properties and reactivity of the new
379 compounds, computational calculations on both imines were carried out. Since (a) the X-ray crystal
380 structures and the NMR studies described above confirmed that imines 1 and 2 adopted the (E) form in
381 the solid state and also in solution and, (b) the use of molecular models showed that for isomers (types c
382 and d in Fig. S1†), with the imine in the syn (Z) form, the proximity of the C5H4 rings would introduce
383 strong steric hindrance that may reduce their stability, only types a and b isomers of the two aldimines
384 were used in the computational studies.
385 All the calculations were carried out using the B3LYP hybrid functional35 and the LANL2DZ36a,b (for
386 Fe and Re) and 6-31G*36c,d (for the remaining atoms) basis set implemented in Gaussian 03
387 software.37 Geometries of the E-isomers of compounds 1 and 2 with different arrangements of the
388 “FeCp” and “Re(CO)3” units (types a and b in Fig. S1†) were optimized without imposing any
389 restriction. Final atomic coordinates of the optimized geometries are included in the ESI†
390 (Coordinates.xyz file). Bond lengths and angles of isomers 1a and 2b were consistent with those
391 obtained from X-ray crystal structures (described above).
392 A comparison of the calculated values of the total energy (ET) obtained for the pairs (1a and 1b) and (2a
393 and 2b) (Table S1†) revealed that in vacuum, the ET values of isomers (1b and 2b) with the syn
394 orientation of the Fe(Cp) and Re(CO)3 moieties were slightly smaller than of their anti analogues (1a
395 and 2a, respectively) [ET (for 1a) – ET (for 1b) = 1.4 kcal mol−1 and ET (for 2a) – ET (for 2b) = 0.8
396 kcal mol−1]. In CH2Cl2 the difference between the ET values of the two isomers 2a and 2b decreased to

397 0.2 kcal mol−1, while for the imine [(η5-C5H5)Fe {(η5-C5H4)-CHvN-(η5-C5H4)}Re(CO)3] the total
398 energy of the anti isomer 1a was found to be 2.7 kcal mol−1 higher than that of 1b.
399 In order to get further information about the stability of the four isomers, their free energies were also
400 calculated (Table S1†). The results obtained in vacuum revealed that for 1 the anti isomer (1a) is 1.58
401 kcal mol−1 more stable than its syn analogue (1b), while for the aldimine 2, the trend is just the
402 opposite. Moreover, the free energies increase according to the sequence 1a <2b <2a <1b, in vacuum,
403 thus indicating a decrease in the stability of the four isomers. When the calculations were carried out
404 taking into account the effect produced by the solvent (CH2Cl2), the calculated free energies followed
405 the same trend, showing again that isomers 1a and 2b (which are found in the crystal structures) are
406 more stable than their corresponding partners (1b and 2a, respectively) and the differences ΔGr, defined
407 as ΔG (of isomer 1b, 2a or 2b) − ΔG (of 1a, the most stable isomer of the set), in CH2Cl2 were higher
408 than those in vacuum (Table 4). According to the calculation compound 1a is expected to be more stable
409 in CH2Cl2 than 2b. However, the NMR studies revealed that 1a hydrolysed slowly in CDCl3 and also in
410 DMSO-d6. This could be due to the presence of traces of HCl and/or residual water in the deuterated
411 solvents.
412 Frontier orbitals [HOMO−1, HOMO, LUMO and LUMO+1] for the most stable isomer of each product
413 (1a, and 2b) are depicted in Fig. 8. The HOMO−1 of 1a and 2b is similar and located on the ferrocenyl
414 unit. In both cases the HOMO is centered on >CvN– and the ferrocenyl unit, with a minor contribution
415 of the cyrhetrenyl moiety. The oxidation of the two aldimines involves this orbital. For 2b, its energy
416 level is higher than that of the HOMO of 1a (Fig. 8); therefore, the removal of one electron is expected
417 to require less energy than for 1a. This explains the differences observed in the cyclic voltammograms
418 shown in Fig. 5A and the shift of the first anodic peak (EIpa) to the more cathodic region (Table 2).
419 Furthermore, comparative analyses of the charge distribution on the metals and imine functional group
420 for isomers 1a and 2b (Table S2†) showed some interesting features. The interchange of the ferrocenyl
421 or cyrhetrenyl arrays in R1-CHvN-R2 of 1a (to give 2b) produces significant variations in the charges of
422 the ipso carbon atoms (C1 and C1′). In contrast, the Mulliken charges on nitrogen are practically
423 identical in both cases and the values are similar to those found in other ferrocenyl Schiff bases with rich
424 and versatile coordination ability to transition metal ions [i.e. Pd(II) and Pt(II)].18,25a This is relevant in
425 view of their potential use as metalloligands to achieve heterotrimetallic complexes containing Fe(II),
426 Re(I) and an additional metal ion Mm+ such as Pd(II) and Pt(II) among others. However, it should be
427 noted that in 2b, the imine nitrogen is not as accessible as in 1a due to steric hindrance.
428 In order to elucidate the origin of the bands detected in the UV-vis spectra in the range 300–500 nm, we
429 decided to undertake a study based on time-dependent DFT (TD-DFT) methodology38 to achieve the
430 assignments of the bands and to confirm the existence of an absorption band at around 380 nm not
431 observed in the UV-vis spectrum of 1. After the optimization of the geometries in vacuum, the
432 excitation energies and the oscillator strengths were calculated in CH2Cl2 solution (Table S3†). The

433 calculated absorption spectra for the two pairs of isomers under study (1a, 1b) and (2a, 2b) are presented
434 in Fig. S10.†
435 The computational results obtained revealed that the main absorption bands arise from a combination of
436 several monoelectronic transitions, of which those with greater contributions are presented in Table S3.†
437 For instance, the band that appears in the range 460–500 nm mainly involves three (for 1a) or two
438 monoelectronic transitions between MO mainly centred on Fe(II), while that observed in the
439 experimental UVvis spectrum of 2b at 383 nm results from the HOMO →LUMO transition, and in both
440 there is a contribution of the cyrhetrenyl unit. Although for 1a, the existence of an absorption band at
441 around 380 nm was not as evident as for 2a, it showed emission after excitation at the same wavelength
442 as for 2b (λexc. = 385 nm). This suggested that 1a might also exhibit electronic transitions at around 380
443 nm. The computational studies confirmed this hypothesis and the presence of an absorption band at
444 λcalc. = 387.2 nm that arises from two main monoelectronic transitions: the HOMO → LUMO (as for
445 2b) and the HOMO−1 → LUMO+3.
446 The experimental UV-vis spectra (Fig. 6) also exhibited two intense and broad bands at lower
447 wavelengths (λ < 350 nm), and according to these computational studies, they result from a large
448 number of monoelectronic transitions that take place in a narrow range of energies (Table S3 and Fig.
449 S10†), of which one of those with greater weight (81% for 1a and 82% for 2b) is the HOMO−2 →
450 LUMO. For 1a this transition leads to an absorption band at λcalc. = 312 nm, while for 2b it appears
451 slightly shifted (ca. 11 nm) to lower energies (λcalc. = 323 nm).
452 Biological studies. Due to increasing interest on organometallic compounds in new drug design, and
453 especially in cancer therapy, in vitro studies on the effect produced by aldimines 1 and 2 on two human
454 breast cancer cell lines [MCF7 and MDA-MB231] and the cisplatin resistant HCT-116 colon cell line
455 were also carried out. In these studies cisplatin was also used as the positive control under identical
456 experimental conditions. A summary of the results obtained for the inhibition concentrations (IC50 in
457 μM) is presented in Table 5 and Fig. 9 and viability plots are shown Fig. S11.†
458 The comparison of results reveals that (a) compound 1 is clearly less active than 2; and (b) aldimine 2
459 showed a cytotoxic effect similar to that of cisplatin in MCF7, but it resulted ca. two times more potent
460 on the triple negative (ER, PR and no HER2 over expression) MDA-MB231 cell line. In view of this,
461 we also evaluated their activity on the cisplatin resistant HCT-116 adenocarcinoma colon cell line. As
462 shown in Table 5 and Fig. S12† compound 2 had a greater inhibitory growth effect than the reference
463 drug, while 1 did not show any relevant activity (IC50 > 30 μM).
464 A parallel study of the antiproliferative effect of the compounds on the normal and non-tumoral human
465 skin fibroblast BJ cell lines was also carried out. The results, presented in Table 5 and Fig. S12† show
466 that the cytotoxicity of the compounds increases according to the sequence 1 < cisplatin ≤ 2. Although
467 compound 2 has an inhibition growth potency on the BJ cell line quite similar to that of cisplatin, it is
468 particularly attractive due to (a) its remarkable stability in the solid state and also in solution; (b) its
469 cytotoxic potency that is comparable to (in MCF7) or even greater (in MDA-MB231 and HCT116) than

470 that of cisplatin; and (c) the fact that it does not contain Pt(II) and consequently might not produce the
471 typical and undesirable side effects of the conventional platinumbased drugs used clinically.39
472

CONCLUSIONS

Two new and isomeric aldimines R1-CHvN-R2 [with R1 = ferrocenyl and R2 = cyrhetrenyl (1) or vice versa (2)] have been prepared and characterized in the solid state as well as in solution. The interchange of the position of the two organometallic arrays in the R1-CHvN-R2 backbones produces significant changes in their structures, the assembly of the molecules in the crystals, their stability, their electrochemical and photophysical properties and also their biological activity. In particular, and despite the formal similarity of 1 and 2 and the fact that both imines adopt the E form in the solid state, in 1 the "FeCp" and "Re(CO)3" arrays are in an anti disposition, while in 2, they are in syn. This affects the type of assembly of the molecules and the intermolecular interactions. We have also proved that aldimine 2 is less prone to hydrolyse and more proclive to undergo the first one electron oxidation process than 1.
The results obtained from the theoretical calculations have allowed us not only to compare (a) the stability of the two isomers of these products with the imine in the E form and differing in the relative orientation of the "Fe(Cp)" and Re (CO)3 units in vacuum and in CH2Cl2, (b) the effect produced by the interchange of the substituents on electronic delocalization and charge distribution and (c) the different electrochemical behaviour, but also to assign the main monoelectronic transitions and the main absorptions bands observed in their UV-vis spectra.
The new hybrid imines exhibit luminescence in CH2Cl2 at 298 K. These findings together with the results obtained from their in vitro studies on their antiproliferative effect on the three human cancer cell lines [breast (MDA-MB231 and MCF7) and colon (HCT-116)] and non-tumoral BJ cells increase the value of these products as a novel type of multifunctional compound, due to their electrochemical behaviour, emissive properties or antitumor activity. Among the two new products presented here, compound 2, with remarkable stability in DMSO and also in DMSO-d6 : water mixtures, appears to be an excellent candidate for further work mainly centred on its cytotoxic activity against other cancer cell lines (i.e., lung, ovarian, etc.), its mechanism of action, and also its potential as an theranostic agent.40
Besides this, both imines have additional interest as building blocks and especially as metallo-ligands to other transition metal ions Mm+ such as Pt(II), Pd(II), and Ru(II), to achieve heterotrimetallic compounds with three metal centres [Fe(II), Re(I) and Mm+] and "potentially bioactive units", which are attractive not only in view of their potential interest in new drug design and development or biotechnology, but also in other emerging fields, such as cooperative catalysis.

EXPERIMENTAL

General remarks

[Re{(η5-C5H4)-CHO}(CO)3] and the amines [Re{(η5-C5H4)-NH2} (CO)3] and [{(η5-C5H5)Fe(η5-C5H4)-NH2}(CO)3] were prepared as described previously.41–43 Ferrocene (98%) and errocenecarboxaldehyde (98%) were obtained from Aldrich and used as received. The solvents (CH2Cl2, hexane and toluene) were obtained commercially and were purified using standard methods.44 All manipulations were conducted under an N2 atmosphere using Schlenk techniques. High resolution mass spectra (HRMS) were recorded at the Servei de Espectrometría de Masses (Univ. Barcelona) using a LC/MSD-TOF Agilent Technologies instrument and electron impact (EI) mass spectra were obtained on a Shimadzu GC-MS spectrometer (70 eV) at the Laboratorio de Servicios Analíticos (Pontificia Universidad Católica de Valparaíso). Infrared spectra of 1 and 2 were obtained using a Nicolet 400 FTIR instrument with KBr pellets. UV-visible (UV-vis) spectra of 1.0 × 10−4 M solutions of the compounds in CH2Cl2 were recorded on a Cary 100 scan Varian UV spectrometer at 298 K. Emission spectra of CH2Cl2 solutions of 1 and 2 were obtained on a Horiba Jobin–Yvon SPEX Nanolog-TM spectrofluorimeter at 298 K.
Routine 1H and 13C{1H} NMR spectra were recorded at 298 K on a Bruker Fourier 300 or a Mercury 400 MHz instrument. High resolution 1H-NMR spectroscopy and two dimensional NMR experiments were carried out using Bruker 400 Avance III HD equipment. Except where quoted, the solvent used for NMR studies was CDCl3 (99.9%) and SiMe4 was the internal reference. The assignment of signals detected in the 1H and 13C{1H} NMR spectra was achieved with the aid of two dimensional [1H–1H] nuclear Overhauser effect spectroscopy (NOESY) and [1H–13C] heteronuclear multiple-bond correlation spectroscopy (HMBC) experiments. NMR data are presented in the characterization section of each compound. Chemical shifts (δ) are given in ppm and the coupling constants (J) in Hz, the assignment of the resonances observed refers to the labelling patterns presented in Scheme S1† and the abbreviations for the multiplicities of the signals are s (singlet) and t (triplet). 1H-NMR studies of compounds 1 and 2 in acetonitrile-d3 (Fig. S6†) and DMSO-d6 (Fig. S7 and S8†) at 298 K and of 1 in DMSO-d6 : D2O (4 : 1) (Fig. S9†) were also undertaken in order to evaluate the stability of the compounds in the solvents used in the electrochemical studies and in the biological studies.

Preparation of the compounds

Synthesis of compound [(η5-C5H5)Fe{(η5-C5H4)-CHvN-(η5-C5H4)}Re(CO)3] (1). To a solution of [Re{(η5-C5H4)-NH2}(CO)3 (122.7 mg, 3.5 × 10−4 mol) in 20 mL dry toluene, [(η5-C5H5)Fe{(η5-

C5H4CHO)}] (75.0 mg, 3.5 × 10−4 mol) and 4 Å molecular sieves (ca. 2.1 g) were added. The flask containing the resulting mixture was connected to Dean–Stark apparatus and a condenser and then the reaction mixture was refluxed for 24 h. After this period, the solvent was removed under vacuum giving a red solid that was later on crystallized from CH2Cl2/hexane at −18 °C to give orange crystals of 1 (yield: 153.2 mg, 2.8 × 10−4 mol, 80%). Characterization data: Mass spectrum: HRMS (m/z): 547.9945, calc. for: C19H15FeNO3Re: 547.9954; EIMS (based on 187Re) m/z: 547 [M+], 518 [M+−CO], 491 [M+−2CO], 463 [M+−3CO]. IR selected data (KBr; cm−1): 2010[ν(CO)], 1931 [ν(CO)] and 1613[ν(CvN)]. 1H NMR (400 MHz) δ: 8.29 (s, 1 H, –CHvN–), 5.40 [t, 2H, 3J = 2.3, (H2 and H5)]; 5.23 [t, 2H, 3J = 2.3, (H3 and H4)], 4.71 [t, 2H, 3J = 1.9, (H2 and H5)], 4.52 [t, 2H, 3J = 1.9, (H3 and H4)] and 4.24 (s, 5H, Cp). 13C NMR (75 MHz) δ: 194.5 (CO); 166.6 (>CHvN–); 129.4 (C1); 81.5 (C2 and C5); 78.9 (C1); 76.5 (C3 and C4); 72.2 (C2 and C5); 69.7 (Cp); and 69.5 (C3 and C4).
Synthesis of compound [(η5-C5H5)Fe{(η5-C5H4)-NvCH-(η5-C5H4)}Re(CO)3 (2). [Re{(η5-C5H4)-CHO}(CO)3] (75.0 mg, 2.1. × 10−4 mol) was added to a solution of [(η5-C5H5)Fe{(η5-C5H4)-NH2}] (41.5 mg, 2.1 × 10−4 mol) in 20 mL dry toluene. The mixture was refluxed for 12 h and after this period, the solvent was pumped off giving a red solid, which was later on crystallized by slow evaporation at −18 °C of a CH2Cl2 solution layered with n-hexane (yield: 96.2 mg, 1.7 × 10−4 mol, 85%). Characterization data: Mass spectrum: HRMS (m/z): 547.9939, calc. for: C19H15FeNO3Re: 547.9954; EIMS (based on 187Re) m/z: 547 [M+], 518 [M+−CO], 491 [M+−2CO], 464 [M+−3CO]. IR selected data (KBr; cm−1): 2015[ν(CO)], 1932 [ν(CO)] and 1610[ν(CvN)]. 1H NMR (400 MHz) δ:8.18 (s, 1H, –CHvN–), 5.93 [t, 2H, 3J = 2.2, (H2 and H5)], 5.40 [t, 2H, 3J = 2.2, (H3 and H4)], 4.49 [t, 2H, 3J = 1.8, (H2 and H5)], 4.25 [t, 2H, 3J = 1.8, (H3 and H4)] and 4.20 (s, 5H, Cp). 13C NMR (75 MHz) δ: 193.2 (CO); 148.9 (>CvN–); 104.1 (C1); 101.1 (C1); 85.3 (C2 and C5), 84.70 (C3 and C4); 69.7 (Cp); 67.7 (C2 and C5) and 62.8 (C3 and C4).

Crystallography

A red prism-like specimen of 1 or a red plate-like crystal of 2 (sizes in Table 6) was selected and mounted on a D8 Venture system equipped with a multilayer monochromator and a Mo microfocus (λ = 0.71073 Å). The frames were integrated with the Bruker SAINT software package using a narrow-frame algorithm. The integration of the data using an orthorhombic (for 1) and a triclinic unit cell (for 2) yielded a total of 21 377 (for 1) and 37 637 (for 2) reflections to a maximum θ = 28.30° (for 1) or 30.57° (for 2) (0.75 Å and 0.70 Å resolution, respectively). For 1, 4125 were independent (average redundancy 5.182, completeness = 99.7%, Rint = 5.94%, Rsig = 4.85% and 3094 (75.01%) were greater than 2 σ(F2)), while for 2, 5064 reflections were independent (average redundancy 7.432, completeness = 99.8%, Rint = 3.06%, Rsig = 1.91% and 4758 (93.96%) were greater than 2 σ(F2)). The final cell constants and volumes for 1 and 2 (Table 6) are based upon the refinement of XYZ centroids of

reflections above 20 σ(I). Data were corrected for absorption effects using the multi-scan method (SADABS). The calculated minimum and maximum transmission coefficients (based on the crystal size) were 0.5655 and 0.7457 for 1 and 0.5529 and 0.7461 for 2.

The structures were solved and refined using the SHELXTL software package45 using the Pbcn (with Z = 8, for 1) and the P1¯ (Z = 2, for 2) space group for the formula unit C19H14FeNO3Re. The final anisotropic full-matrix least-squares refinement on F2 with 226 variables converged at R1 = 3.36 (for 1) and 1.50% (for 2) for the observed data, and wR2 = 6.01% (for 1) and 3.17% (for 2) for all data. The largest peak in the final difference electron density synthesis was 0.888 e Å−3 (in 1) and 0.691 e Å−3 (in 2) and the largest hole was −1.093 e Å−3 (in 1) and −1.031 e Å−3 (in 2) with RMS deviations of 0.196 and 0.118 e Å−3 for 1 and 2, respectively. Further detail concerning the resolution and refinement of the two crystal structures is presented in Table 6.

CCDC 1576497 (for 1) and 1576498 (for 2)† contain the supplementary crystallographic data for this paper.

Electrochemical studies

Cyclic voltammetric (CV) studies were carried out at room temperature using a potentiostat (Metrohm Autolab potentiostat) in a three-electrode cell. Each complex was dissolved in acetonitrile containing 0.1 mol L−1 tetrabutylammoniumhexafluorophosphate (Bu4N)[PF6], as the supporting electrolyte to give 10−3 mol L−1 final concentration. A platinum 2 mm working electrode and a platinum coil counter electrode were used. The reference electrode contained a silver wire with 10 mM silver nitrate in (Bu4N)[PF6] electrolyte solution.

The working electrode was polished with 0.3 and 0.05 μm alumina slurries, rinsed with distilled water (18 MΩ cm) and acetone, and dried prior to use. All electrolyte solutions were thoroughly pre-purged using purified nitrogen gas before use. The measurements were carried out at a scan rate of 0.25 V s−1. The ferrocene/ferricinium (Fc/Fc+) couple served as the internal reference and appeared at +89 mV (vs Ag/Ag+) for each experiment.

Computational studies

DFT calculations were carried out using Gaussian 03 software, 37 with the B3LYP functional.35 The basis set was chosen as follows: LANL2DZ36a,b for Fe and Re and 6-31G*36c,d (including polarization functions for non-hydrogen atoms) for C, N, O and H. All molecular structures were optimized without symmetry constraints and characterized as minima by vibrational analysis. Solvent effects have been included using the CPCM method.46

615 **Biological studies**

616

617 Cell culture. Breast cancer (MCF7 and MDA-MB231) cells (from European Collection of Cell Cultures,
618 ECACC) and colon adenocarcinoma (HCT-116) cells (from the American Type Culture Collection)
619 were used in all the experiments. Cells were grown as a monolayer culture in minimum essential
620 medium (DMEM with L-glutamine, without glucose and without sodium pyruvate) in the presence of
621 10% heat-inactivated fetal calf serum, 10 mM of D-glucose and 0.1% streptomycin/penicillin under
622 standard culture conditions.
623 Cell viability assays. For these studies, the compounds were dissolved in 100% DMSO at 50 mM as
624 stock solution; then, serial dilutions were prepared in DMSO (1 : 1) (in this way the DMSO
625 concentration in cell media was always the same); and finally, 1 : 500 dilutions of the serial dilutions of
626 the compounds in cell media were prepared. The assay was performed as described by Givens et al.47
627 In brief, MDA-MB231 and MCF7 cells were plated at 5000 cells per well and 10 000 cells per well,
628 respectively, in 100 Ml media in tissue culture 96 well plates (Cultek). After 24 h, the medium was
629 replaced by 100 μL per well of serial dilution of drugs. Each point concentration was run in triplicate.
630 Reagent blanks, containing media plus the colorimetric reagent without cells, were run on each plate.
631 Blank values were subtracted from test values and were routinely 5–10% of uninhibited control values.
632 The plates were incubated for 72 h. Hexosaminidase activity was measured according to the following
633 protocol: the media containing the cells were removed and the cells were washed once with PBS; 60 μL
634 substrate solution (p-nitrophenol-N-acetyl-β-D-glucosamide 7.5 mM [Sigma N-9376], sodium citrate
635 0.1 M, pH = 5.0, 0.25% Triton X-100) was added to each well and incubated at 37 °C for 1–2 hours;
636 after this incubation time, a bright yellow color appeared; then, the plates could be developed by adding
637 90 μL developer solution (Glycine 50 mM, pH = 10.4; EDTA 5 mM); and absorbance was recorded at
638 410 nm.
639 The human skin fibroblast cell line BJ was cultured in DMEM in the presence of 10% FBS, 12.5 mM
640 DE-glucose, 4 mM glutamine, 5 mN pyruvate and 0.5 streptomycin/penicillin. All the cells were
641 incubated under standard conditions (humidified air with 5% CO2 at 37 °C). The cells were passaged at
642 confluence by washing once with cation-free HBSS followed by a 3 minute incubation with trypsin ([0.5
643 μg mL−1]/EDTA [0.2 μg mL−1]) (Gibco-BRL, 15400054) solution in HBSS at 37 °C, and transferred to
644 its medium. Prior to seeding at a defined cell concentration, the cells were recovered from the medium
645 by centrifugation and counted. For proliferation studies, the cells were plated at 5000 cells per well in
646 100 μL media in tissue culture 96 well plates (Cultek). After 24 h, the media were replaced by 100 μL
647 per well of serial dilution 1 : 2 of compounds 1 and 2.
648 For comparison purposes, a parallel study with cisplatin was also carried out under identical conditions.
649 Reagent blanks, containing media plus colorimetric reagent without cells, were run on each plate. Blank
650 values were subtracted from test values and were routinely 5–10% of uninhibited control values. The
651 plates were incubated for 72 h. Hexosaminidase activity was measured according to the following

652 protocol: the media containing the cells were removed and the cells were washed once with PBS; 60 µL
653 of substrate solution (p-nitrophenol-N-acetyl-beta-D-glucosamide 7.5 mM [Sigma N-9376], sodium
654 citrate 0.1 M, pH 5.0, 0.25% Triton X-100) was added to each well and incubated at 37 °C for 1–2
655 hours; after this incubation time, a bright yellow color appeared; then, the plates could be developed by
656 adding 90 µL developer solution (Glycine 50 mM, pH 10.4; EDTA 5 mM); and absorbance was
657 recorded at 410 nm.
658

ACKNOWLEDGEMENTS

H. K. and R. A. acknowledge FONDECYT-Chile (Projects 1150601 and 11130443), FONDEQUIP EQM 130154 and D. I. Pontificia Universidad Católica de Valparaíso. J. O. is grateful to CONICYT-PFCHA for a doctoral scholarship number 21170802 and D.I.-PUCV. C. P. S. is grateful to Postdoc DICYT code 021740PI, Vicerrectoría de investigación, Desarrollo e investigación. This work was also supported by the Ministerio de Economia y Competitividad of Spain [grant number CTQ2015-65040-P (subprograma BQU)].

668 **REFERENCES**

669

670 1 (a) J. Pombeiro and J. A. McCleverty, Molecular Electrochemistry of Inorganic, Bioinorganic
671 and Organometallic Compounds, Springer Science & Business Media, 2012; (b) D. M.
672 Roundhill and J. P. Kackler, Optoelectronic properties of Inorganic Compounds, Springer
673 Science & Business Media, 2013.

674 2 S. Di Bella, Chem. Soc. Rev., 2001, 30, 355–366.

675 3 (a) Homo and Heterobimetallic Complexes in Catalysis: Cooperative Catalysts, ed. P. Kalk,
676 Springer, 2016; (b) M. H. Perez-Temprano, J. A. Casares and P. Espinet, Chem. – Eur. J., 2012,
677 18, 1864–1884.

678 4 Selected articles on heterobimetallic compounds with outstanding biological activity: (a) Y. F.
679 Mui, J. Fernandez-Gallardo, B. T. Elie, A. Gubran, I. Maluenda, M. Sanau, O. Navarro and M.
680 Contel, Organometallics, 2016, 35, 1218–1227; (b) M. Wenzel, A. De Almeida, E. Bigaeva, P.
681 Kavanagh, M. Picquet, P. Le Gendre, E. Bodio and A. Casini, Inorg. Chem., 2016, 55, 2544–
682 2557.

683 5 L. Ouahab, Multifunctional Molecular Materials, Pan Sanford. Publish, Singapur, 2013.

684 6 Bioorganometallic Chemistry: Applications in Drug Discovery, Biocatalysys, and Imaging, ed.
685 G. Jaouen and M. Le Salmain, Wiley-VCH, Weinheim, Germany, 2015.

686 7 For a general overview on the potential of organometallic compounds in drug design, medicinal
687 chemistry and therapeutic uses see for instance: (a) B. Biersack and R. Schobert, Adv. Exp.
688 Med. Biol., 2016, 893, 211–224; (b) T. S. Morals and M. H. Garcia, Adv. Organomet. Chem.
689 Catal., 2014, 581–587; (c) P. Martins, M. Marqués, L. Coito, J. Pombeiro, P. Viana-Baptista and
690 A. R. Fernandes, Anti-Cancer Agent Med. Ther., 2014, 14, 1199–1212; (d) D.-L. Ma, D. S.-H.
691 Chan and C.-H. Leung, Acc. Chem. Res., 2014, 47, 3613–3614; (e) B. Anilammert,
692 Pharmacology, 2012, 651–680; (f) G. Gasser and N. Metzler-Nolte, Curr. Opin. Chem. Biol.,
693 2012, 16, 84–91; (g) N. Chavain and C. Biot, Curr. Med. Chem., 2010, 17, 2729–2745; (h) C.
694 Gaiddon and M. Pfeffer, Eur. J. Inorg. Chem., 2017, 1639–1654; (i) I. Omae, Coord. Chem.
695 Rev., 2014, 280, 84–95; (j) M. Patra, G. Gasser and N. Metzler-Nolte, Dalton Trans., 2012, 41,
696 6350–6358.

697 8 Selected contributions on the utility of organometallic compounds in cell imaging, as bioprobes,
698 selective biosensors or as radiopharmaceuticals: (a) K. K.-W. Lo, Inorganic and Organometallic
699 Transition Metal complexes with Biological Molecules and Living Cells, Academic Press, 2016;

(b) F. L. Thorp-Greenwood, R. G. Balasingham and M. P. Coogan, J. Organomet. Chem., 2012, 714, 12–21; (c) A. Monney and M. Albrecht, Coord. Chem. Rev., 2013, 257, 2420–2433; (d) I. S. Butler, R. P. Kegne-Momo, G. Jaouen, C. Policar and A. Vessières, Appl. Spectrosc. Rev., 2012, 47, 531–549; (e) Z. Lam, K. V. Kong, M. Olivo and W. K. Leong, Analyst, 2016, 141, 1569–1586.

9 (a) P. Stepnicka, Ferrocenes: Ligands, Materials and Biomolecules, Wiley-VCH, Weinheim, Germany, 2008; (b) E. S. Phillips, Ferrocenes: Compounds, Properties, and Applications, Nova Science Publishers, Hauppauge, 2011.

10 (a) F. A. Larik, A. Saeed, T. A. Fattah, U. Muqadar and P. A. Channar, Appl. Organomet. Chem., 2016, 1–22; (b) C. Ornelas, New J. Chem., 2011, 35, 1973–1985; (c) S. S. Braga and A. M. S. Silva, Organometallics, 2013, 32, 5626–5639; (d) D. Astruc, Eur. J. Inorg. Chem., 2017, 6–29.

11 For relevant and recent articles on the utility of Re(I)-carbonyl complexes as sensors, in live cell imaging, or enzyme inhibitors see for instance: (a) L. J. Raszeja, D. Siegmund, A. L. Cordes, J. Guldenhaupt, K. Gerwert, S. Hahn and N. Metzler-Nolte, Chem. Commun., 2017, 905–908; (b) A. Ramdass, V. Sathish, V. Murugesan, P. Thanasekaran, S. Umapathy and S. Rajagopal, RSC Adv., 2015, 5, 38479–38488; (c) D. Can, B. Spingler, P. Schmutz, F. Mendez, P. Raposinho, C. Fernandes, F. Carta, A. Innocenti, I. Santos, C. T. Supuran and R. Alberto, Angew. Chem., Int. Ed., 2012, 51, 3354–3357; (d) A. Leonidova, C. Mari, C. Aebersold and G. Gasser, Organometallics, 2016, 35, 851–854; (e) A. Leonidova and G. Gasser, ACS Chem. Biol., 2014, 9, 2180–2193.

12 S. Clede, F. Lambert, C. Sandt, Z. Gueroui, N. Delsuc, P. Dumas, A. Vessières and C. Policar, Biotechnol. Adv., 2013, 31, 393–395.

13 (a) L. Glans, W. Hu, C. Jost, C. de Kock, P. J. Smith, M. Haukka, H. Bruhn, U. Schatzschneider and E. Nordlander, Dalton Trans., 2012, 41, 6443–6450; (b) R. Arancibia, F. Dubar, B. Pradines, I. Forfar, D. Dive, A. H. Klahn and C. Biot, Med. Chem., 2010, 18, 8085–8091.

14 K. Kowalski, L. Szczupak, S. Saloman, D. Steverding, A. Jablonski, V. Vrcek, A. Hildebrandt, H. Lang and A. Rybarczyk-Pirek, ChemPlusChem, 2017, 82, 303–314.

15 (a) F. Godoy, A. Gómez, N. Agurto, M. Muñoz, R. Segura, C. P. Silva, J. Pavez, J. H. Zagal, A. H. Klahn, M. Fuentealba, A. Ibañez and M. T. Garland, J. Organomet. Chem., 2015, 788, 42–48; (b) R. Arancibia, C. Biot, G. Delanay, P. Roussel, A. Pascual, B. Pradines and A. H. Klahn,

J. Organomet. Chem., 2013, 723, 143–148; (c) P. Toro, A. H. Klahn, B. Pradines, F. Lahoz, A. Pascual, C. Biot and R. Arancibia, Inorg. Chem. Commun., 2013, 35, 126–129.

16 (a) R. Arancibia, A. H. Klahn, M. Lapier, J. D. Maya, A. Ibañez, M. T. Garland, S. Carrere-Kremer, L. Kremer and C. Biot, J. Organomet. Chem., 2014, 755, 1–6; (b) R. Arancibia, C. Quintana, C. Biot, M. E. Medina, S. Carrere-Kremer, L. Kremer and A. H. Klahn, Inorg. Chem. Commun., 2015, 55, 139–142.

17 (a) R. Arancibia, F. Godoy, G. E. Buono-Cuore, A. H. Klahn, E. Gutierrez-Puebla and A. Monge, Polyhedron, 2008, 27, 2421–2425; (b) R. Arancibia, A. H. Klahn, G. E. Buono-Core,E. Gutierrez-Puebla, A. Monge, M. E. Medina, C. Olea-Azar, J. D. Maya and F. Godoy, J. Organomet. Chem., 2011, 696, 3238–3244; (c) R. Arancibia, A. H. Klahn, G. E. Buono-Core, D. Contreras, G. Barriga, C. Olea-Azar, M. Lapier, J. D. Maya, A. Ibañez and M. T. Garland, J. Organomet. Chem., 2013, 743, 49–54; (d) C. Echeverria, V. Romero, R. Arancibia, A. H. Klahn, I. Montorfano, R. Armisen, V. Borgna, F. Simon and R. Ramirez-Tagle, BioMetals, 2016, 29, 743–749.

18 Selected articles on the antitumoral activity of different sorts of imines (including ferrocenylaldimines) and their Pd(II) or Pt(II) complexes on cancer cell lines: (a) J. Albert, R. Bosque, M. Crespo, J. Granell, C. López, R. Cortés, A. González, J. Quirante, C. Calvis, R. Messeguer, L. Baldomà, J. Badía and M. Cascante, Bioorg. Med. Chem., 2013, 21, 4210–4217; (b) C. López, R. Bosque, M. Pujol, J. Simó, E. Sevilla, M. Font-Bardía, R. Messeguer and C. Calvis, Inorganics, 2014, 2, 620–648.

19 (a) D. Talancón, C. López, M. Font-Bardía, T. Calvet, J. Quirante, C. Calvis, R. Messeguer, R. Cortés, M. Cascante, L. Baldomà and J. Badia, J. Inorg. Biochem., 2013, 118, 1–12; (b) R. Cortés, M. Tarrado-Castellarnau, D. Talancón, C. López, W. Link, D. Ruiz, J. J. Centelles, J. Quirante and M. Cascante, Metallomics, 2014, 6, 622–633. 20 C. López, J. Sales, X. Solans and R. Zquiak, J. Chem. Soc., Dalton Trans., 1992, 2321–2328.

21 R. Bosque, C. López, J. Sales, X. Solans and M. Font-Bardía, J. Chem. Soc., Dalton Trans., 1994, 735–745.

22 R. Bosque, C. López, J. Sales and X. Solans, J. Organomet. Chem., 1994, 483, 61–71.

23 See for instance: (a) Comprehensive Organic Chemistry, ed. D. Barton and W. D. Ollis, Pergamon, Oxford, UK, 1979; (b) A. M. Belostotskii, Conformational Concept for Synthetic Chemist's Use: Principles in Lab Exploitation, World Scientific, 2015.

24 C. López, R. Bosque, X. Solans and M. Font-Bardia, New J. Chem., 1996, 20, 1285–1292.

25 (a) S. Pérez, C. López, A. Caubet, R. Bosque, X. Solans, M. Font-Bardía, A. Roig and E. Molins, Organometallics, 2004, 23, 224–236; (b) C. López, R. Bosque, S. Pérez, A. Roig, E. Molins, X. Solans and M. Font-Bardía, J. Organomet. Chem., 2006, 691, 475–484.

26 (a) Cambridge Crystallographic Data Centre (CCDC), [http://www.ccdc.cam.uk/data (accessed on June 2017)]; (b) C. R. Groom, I. J. Bruno, M. P. Lightfoot and S. C. Ward, Acta Crystallogr., Sect. B: Struct. Sci., Cryst. Eng. Mater., 2016, 72, 171–179.

27 T. Cautivo, A. H. Klahn, F. Godoy, C. López, M. Font-Bardía, T. Calvet, E. Gutierrez-Puebla and A. Monge, Organometallics, 2011, 30, 5578–5589.

28 (a) A. Bondi, J. Phys. Chem., 1964, 68, 441–451; (b) S. S. Batsanov, Inorg. Mater., 2001, 37, 871–885.

29 E. R. Brown and J. R. Sandifer, in Physical Methods in Chemistry. Electrochemical Methods, ed. B. W. Rossiter and J. F. Hamilton, Wiley, New York, USA, 1986, ch. 4, vol. 4.

30 R. Bosque, C. López and J. Sales, Inorg. Chim. Acta, 1996, 244, 141–145.

31 J. J. R. Fraústo da Silva and R. J. P. Williams, The Biological Chemistry of Elements: The Inorganic Chemistry of Life, Oxford University Press, Oxford, UK, 2nd edn, 2001.

32 J. Gómez, N. Leiva, R. Arancibia, J. Oyarzo, G. E. Buono-Cuore, A. H. Klahn, V. Artigas, M. Fuentealba, R. Bosque, G. Aullón, C. López, M. Font-Bardía and T. Calvet, J. Organomet. Chem., 2016, 819, 129–137.

33 A. J. Lees, Photophysic of Organometallics, Springer, Heildelberg, Germany, 2010.

34 Comprehensive Coordination Chemistry II: from Biology to Nanotechnology, ed. J. A. Mc.Cleverty and T. J. Meyer, Elsevier, Amsterdam, The Netherlands, 2003.

35 B3LYP. (a) A. D. J. Becke, Chem. Phys., 1993, 98, 5648–5652; (b) C. Lee, W. Yang and R. G. Parr, Phys. Rev. B: Condens. Matter Mater. Phys., 1988, 37, 785–789.

36 (a) W. R. Wadt and P. J. Hay, J. Chem. Phys., 1985, 82, 284–298; (b) P. J. Hay and W. R. Wadt, J. Chem. Phys., 1985, 82, 299–310; (c) P. C. Hariharan and J. A. Pople, Theor. Chim. Acta, 1973, 28, 213–222; (d) M. M. Francl, W. J. Pietro, W. J. Hehre, J. S. Binkley, M. S. Gordon, D. J. DeFrees and J. A. Pople, J. Chem. Phys., 1982, 77, 3654–3665.

37 M. J. Frisch, G. W. Trucks, H. B. Schlegel, G. E. Scuseria, M. A. Robb, J. R. Cheeseman, J. A. Montgomery, T. Vreven, K. N. Kudin, J. C. Burant, J. M. Millam, S. S. Iyengar, J. Tomasi, V.

Barone, B. Mennucci, M. Cossi, G. Scalmani, N. Rega, G. A. Petersson, H. Nakatsuji, M. Hada, M. Ehara, K. Toyota, R. Fukuda, J. Hasegawa, M. Ishida, T. Nakajima, Y. Honda, O. Kitao, H. Nakai, M. Klene, X. Li, J. E. Knox, H. P. Hratchian, J. B. Cross, V. Bakken, C. Adamo, J. Jaramillo, R. Gomperts, R. E. Stratmann, O. Yazyev, A. J. Austin, R. Cammi, C. Pomelli, J. W. Ochterski, P. Y. Ayala, K. Morokuma, G. A. Voth, P. Salvador, J. J. Dannenberg, V. G. Zakrzewski, S. Dapprich, A. D. Daniels, M. C. Strain, O. Farkas, D. K. Malick, A. D. Rabuck, K. Raghavachari, J. B. Foresman, J. V. Ortiz, Q. Cui, A. G. Baboul, S. Clifford, J. Cioslowski, B. B. Stefanov, G. Liu, A. Liashenko, P. Piskorz, I. Komaromi, R. L. Martin, D. J. Fox, T. Keith, M. A. Al-Laham, C. Y. Peng, A. Nanayakkara, M. Challacombe, P. M. W. Gill, B. Johnson, W. Chen, M. W. Wong, C. Gonzalez and J. A. Pople, Gaussian 03 (Revision C.02), Gaussian, Inc., Wallingford, CT, 2004.

38 M. E. Casida, C. Jamorski, K. C. Casida and D. R. Salahub, J. Chem. Phys., 1998, 108, 4439–4449.

39 See for instance: (a) D. Theile, Molecules, 2017, 22, 382; (b) S. Dasari and P. B. Tchounwou, Eur. J. Pharmacol., 2014, 364–378.

40 (a) A. Tiwari, H. K. Patra and J. W. Choi, Advances Theranostic Materials, Wiley, 2015; (b) X. Chen and S. Wong, Cancer Theranostics, Accademic Press, San Diego, USA, 2015.

41 D. Chong, D. Laws, A. Nafady, P. Costa, A. Rheingold, M. Calhorda and W. Geiger, J. Am. Chem. Soc., 2008, 130, 2692–2703.

42 J. Heldt, N. Fischer-Durand, M. Salmain, A. Vessiéres and G. Jaouen, J. Organomet. Chem., 2004, 689, 4775–4782.

43 D. Van Leusen and B. Hessen, Organometallics, 2001, 20, 224–226.

44 D. D. Perrin and W. L. F. Armarego, Purification of Laboratory Chemicals, Butterworth–Heinemann, Oxford, UK, 4th edn, 1996.

45 G. M. Sheldrick, Acta Crystallogr., Sect. A: Found. Adv., 2015, 71, 3–8.

46 M. Cossi, N. Rega, G. Scalmani and V. Barone, J. Comput. Chem., 2003, 24, 669–681.

47 K. T. Givens, S. Kitada, A. K. Chen, J. Rothschiller and D. A. Lee, Invest. Ophthalmol. Visual Sci., 1990, 31, 1856–1862.

821 **Legends to figures**

822

823 **Figure. 1** Representative examples of cyrhetrenes containing appended bioactive units with relevant
824 biological activities.

825

826 **Figure.2** Examples of ferrocenylimines (A and B) with cytotoxic activity and their Pt(II) complexes (C–
827 E) with greater inhibitory growth potency than their corresponding parent ligands. IC50 values for D
828 and E in A549 (lung), MDA-MB231 (breast) or HCT116 (colon) cancer cell lines ranged from 1.5 μM
829 to 10 μM.

830

831 **Chart 1** Chemical formulae of the novel hybrid ferrocenyl/cyrhetrenyl aldimines prepared in this work
832 and the atom labelling scheme.

833

834 **Figure.3** The molecular structure of [(η5-C5H5)Fe{(η5-C5H4)-CHvN-(η5-C5H4)Re(CO)3}] (1).

835

836 **Figure.4**. The molecular structure of [(η5-C5H5)Fe{(η5-C5H4)-NvCH-(η5-C5H4)Re(CO)3}] (2).

837

838 **Figure.5** Cyclic voltammograms of the new aldimines 1 and 2, in the ranges of potentials: −1.20 V ≤ E
839 ≤ 0.50 V (A) and −1.00 V ≤ E ≤ 1.60 V (B), together with the labelling system used for the observed
840 peaks.

841

842 **Figure.6** UV-vis spectra of 10−4 M solutions of aldimines 1 and 2 in CH2Cl2 at 298 K.

843

844 **Figure.7** Emission spectra of 10−4 M solutions of the aldimines 1 and 2 in CH2Cl2 at 298 K upon
845 excitation at λexc. = 477 nm (A) or 383 nm (B).

846

847 **Figure.8** Frontier orbitals of isomers 1a (left) and 2b (right) together with their energies and the values
848 of the HOMO–LUMO gap

849

850 **Figure.9** A comparative plot of the IC50 values (μM) of 2 and cisplatin against the three cancer cell
851 lines used in this study: MCF7 and MDA-MB231 (breast) and HCT-116 (colon) cancer cell lines.

852

853 **FIGURE 1**

854

855

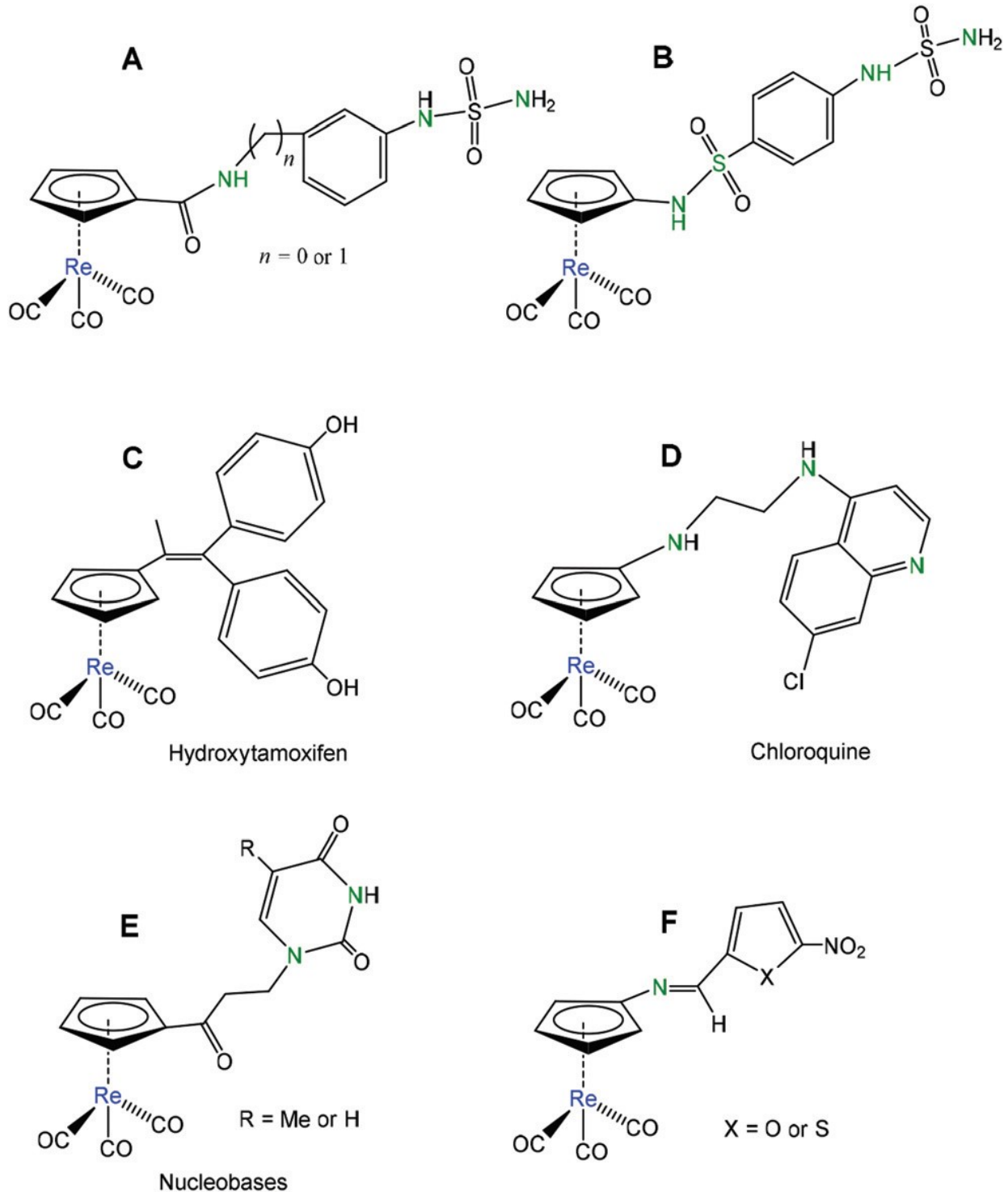

856

857

858

859 **FIGURE 2**

860

861

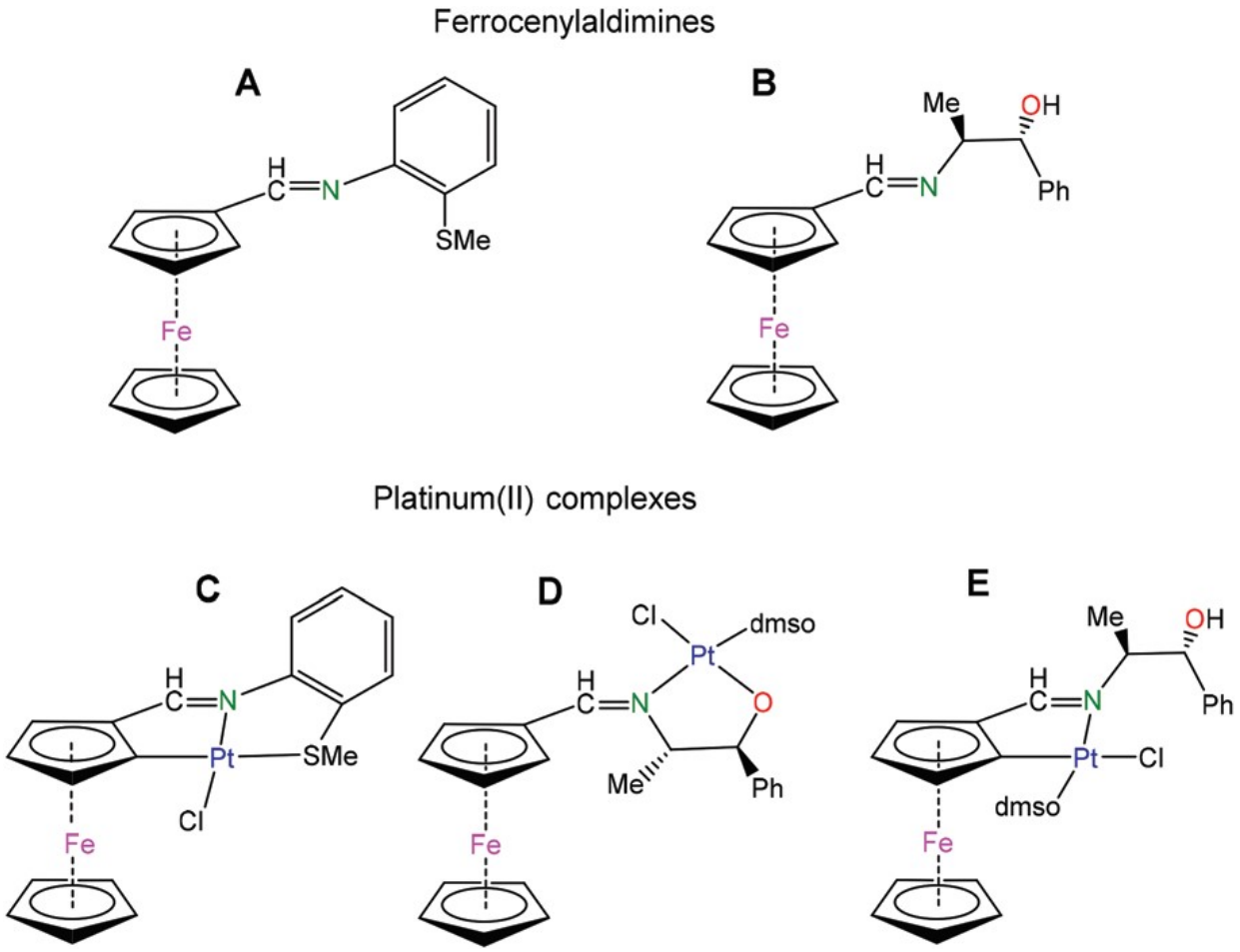

862

863

CHART 1

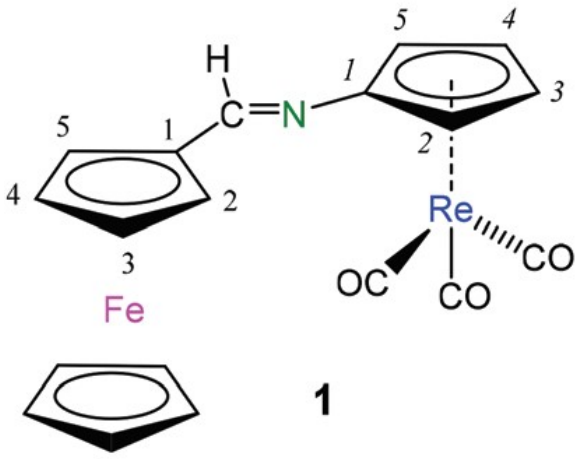

1

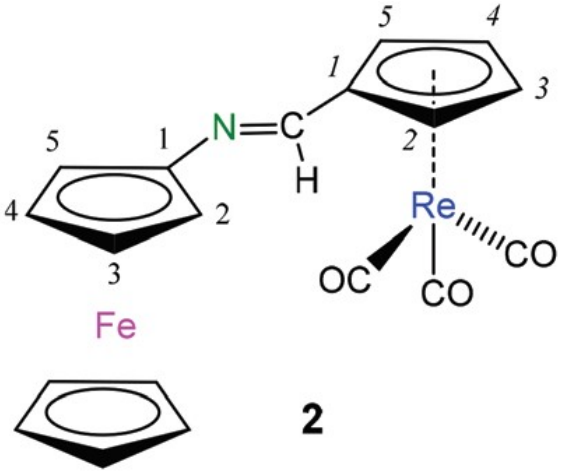

2

FIGURE 3

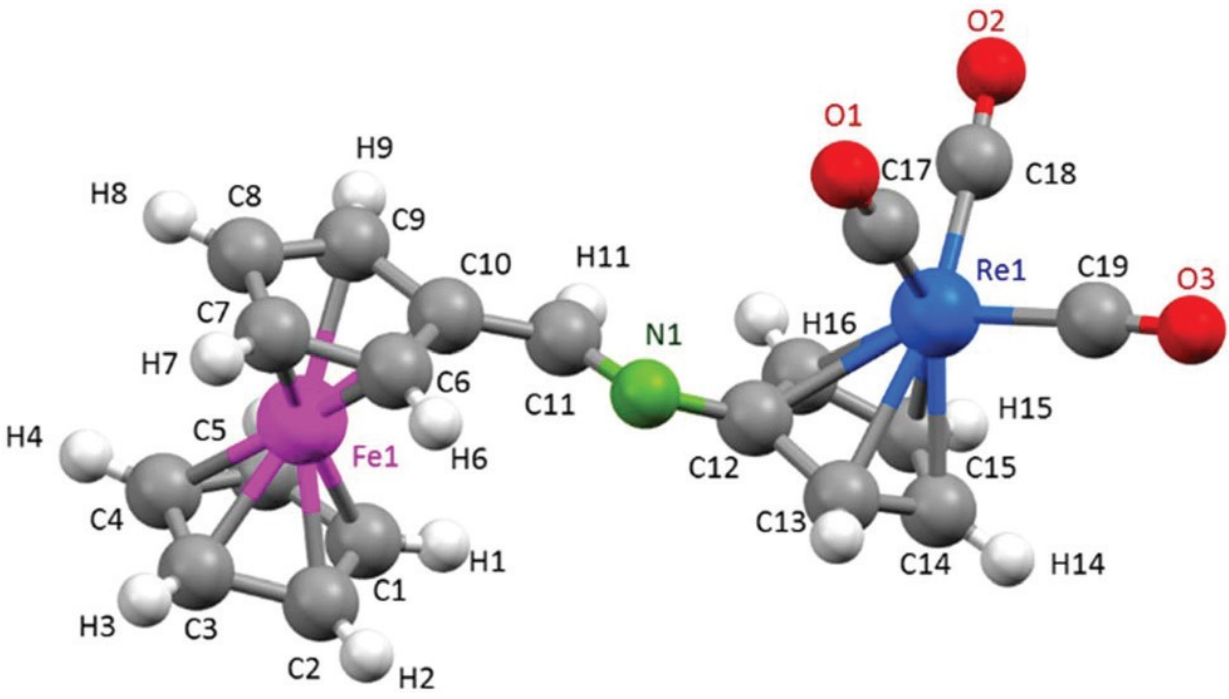
O2
O1
H9
C17
C18
H8
C8
C9
C10
H11
Re1
C19
O3
C7
N1
H16
H7
C6
C11
H15
H4
C5
Fe1
H6
C12
C15
C4
C13
H1
C14
H14
C1
H3
C3
C2
H2

FIGURE 4

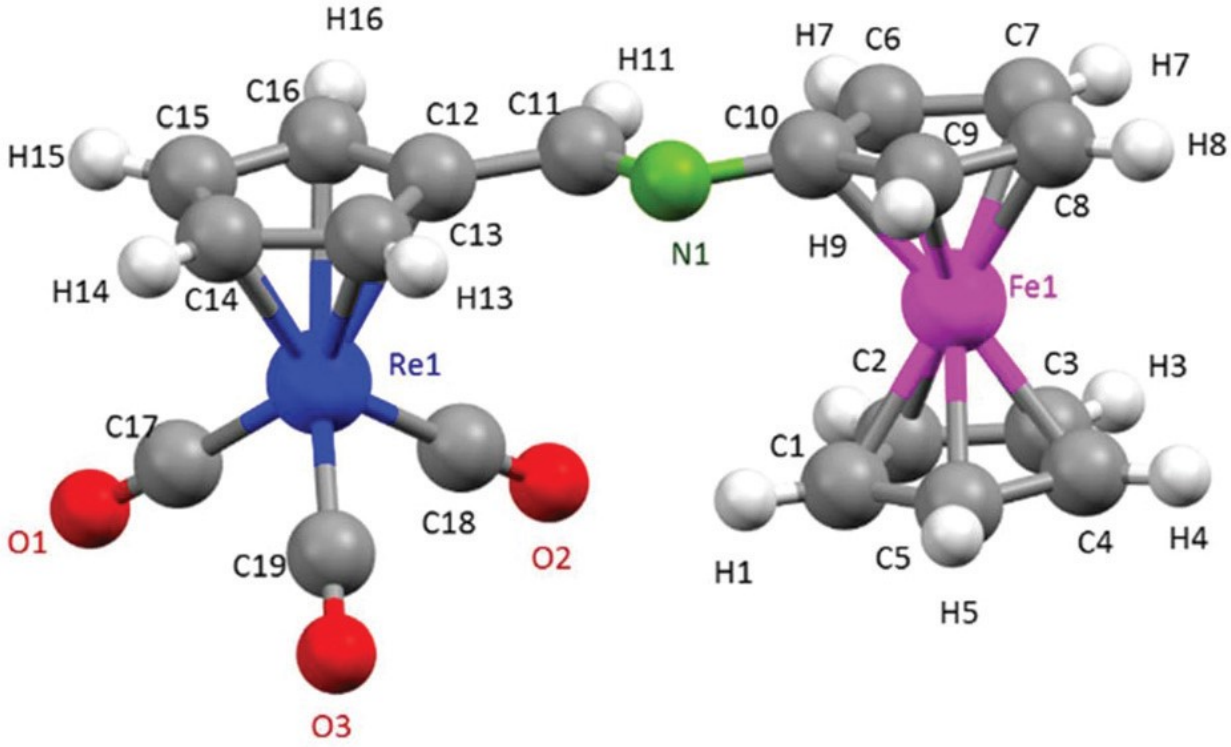
H16
C16
C15
H15
C12
C11
H11
C10
H7
C6
C7
H7
C9
H8
C8
C13
N1
H9
H14
C14
H13
Fe1
Re1
C2
C3
H3
C17
C1
O1
C18
O2
C19
C5
C4
H4
H1
H5
O3

882 **FIGURE 5**

883

884

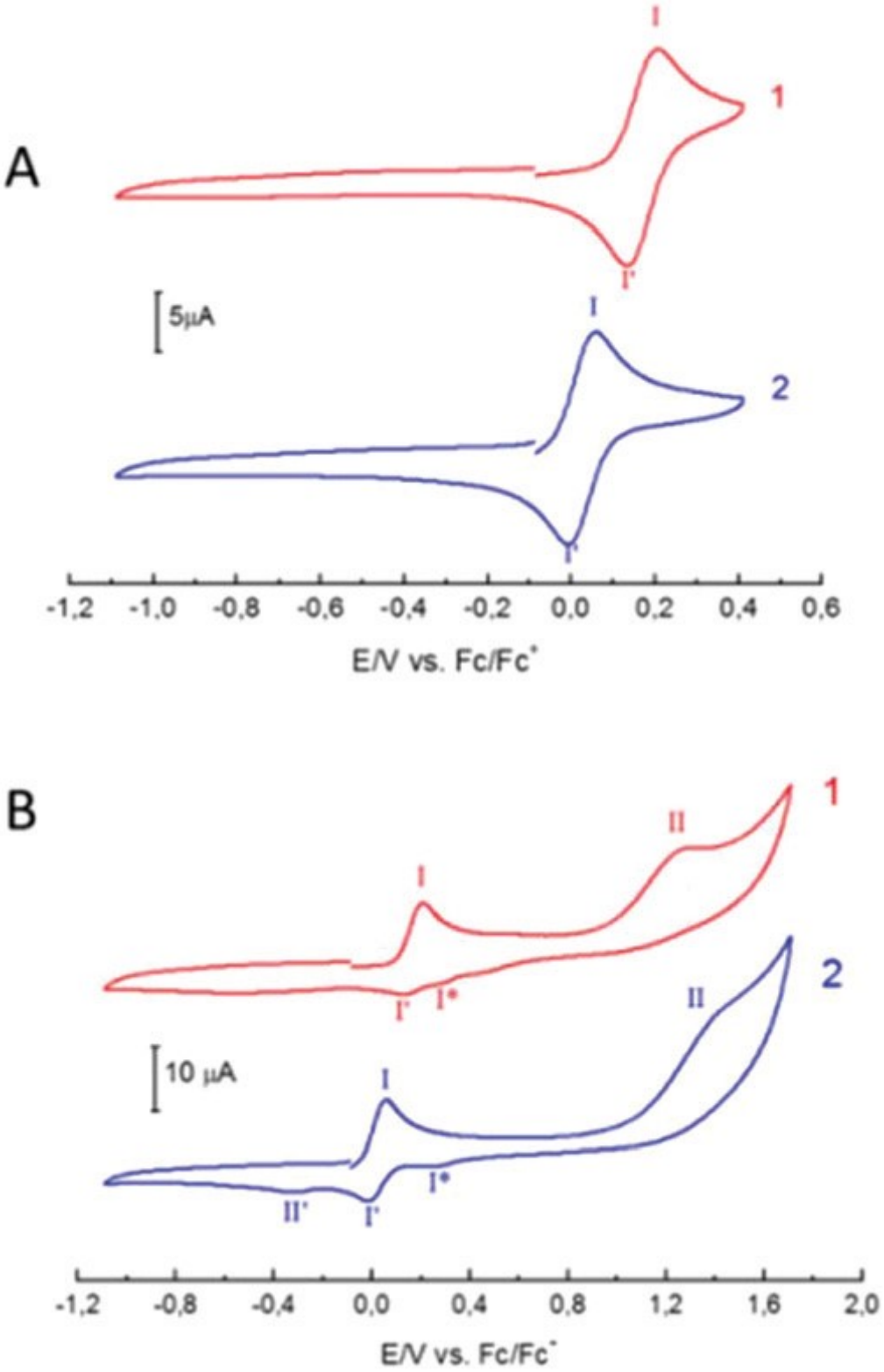

885

886

887 **FIGURE 6**

888

889

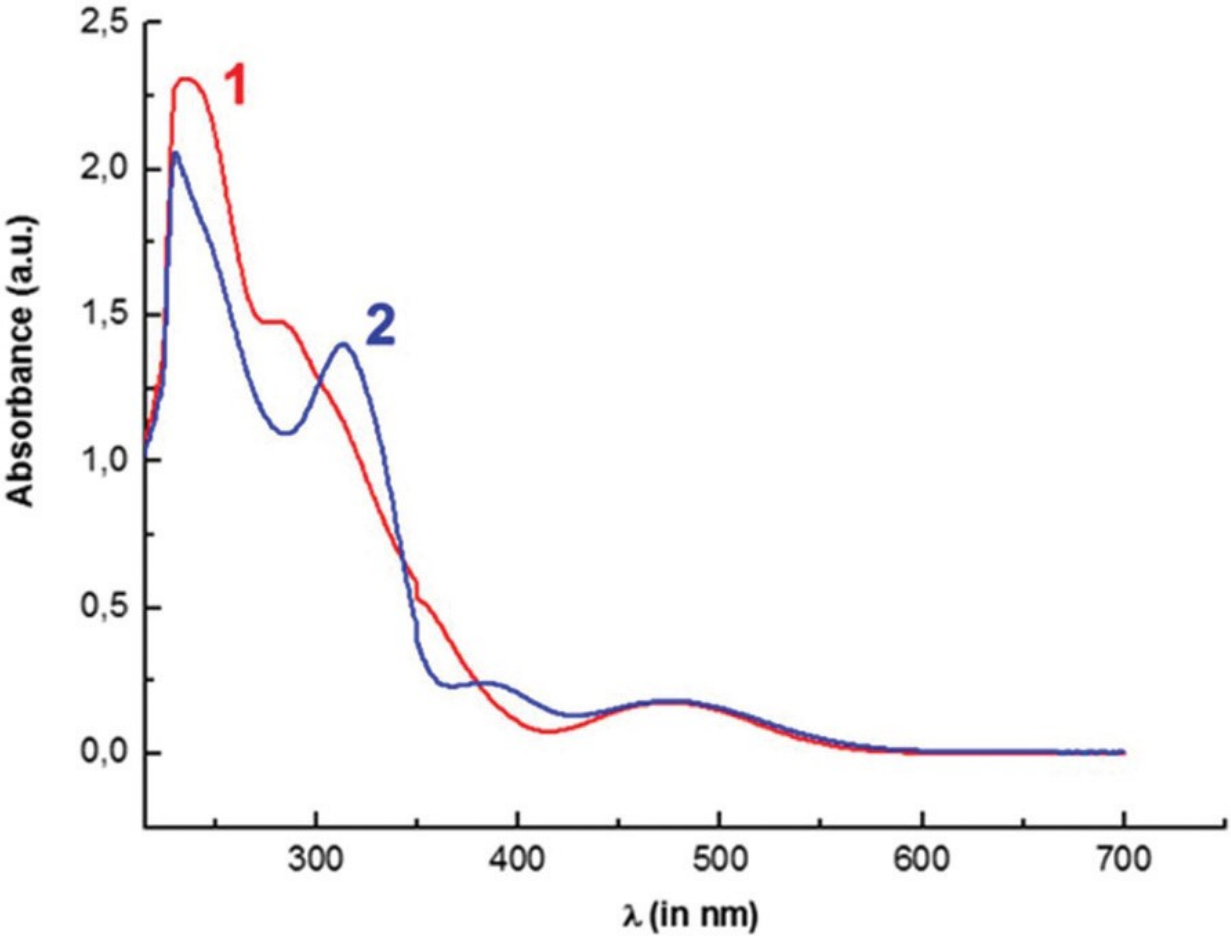

890

891

892 **FIGURE 7**

893

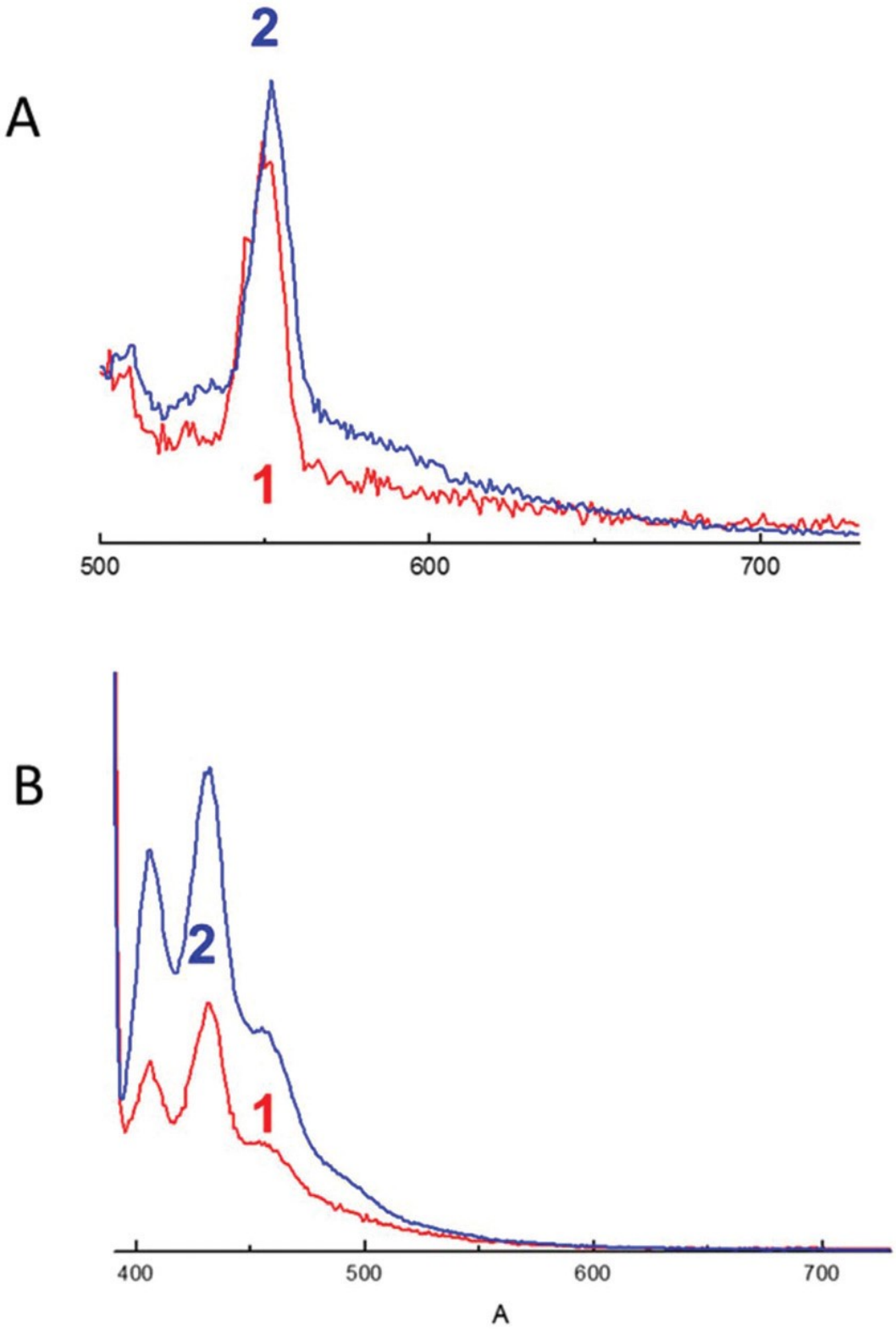

894

895

896 **FIGURE 8**

897

898

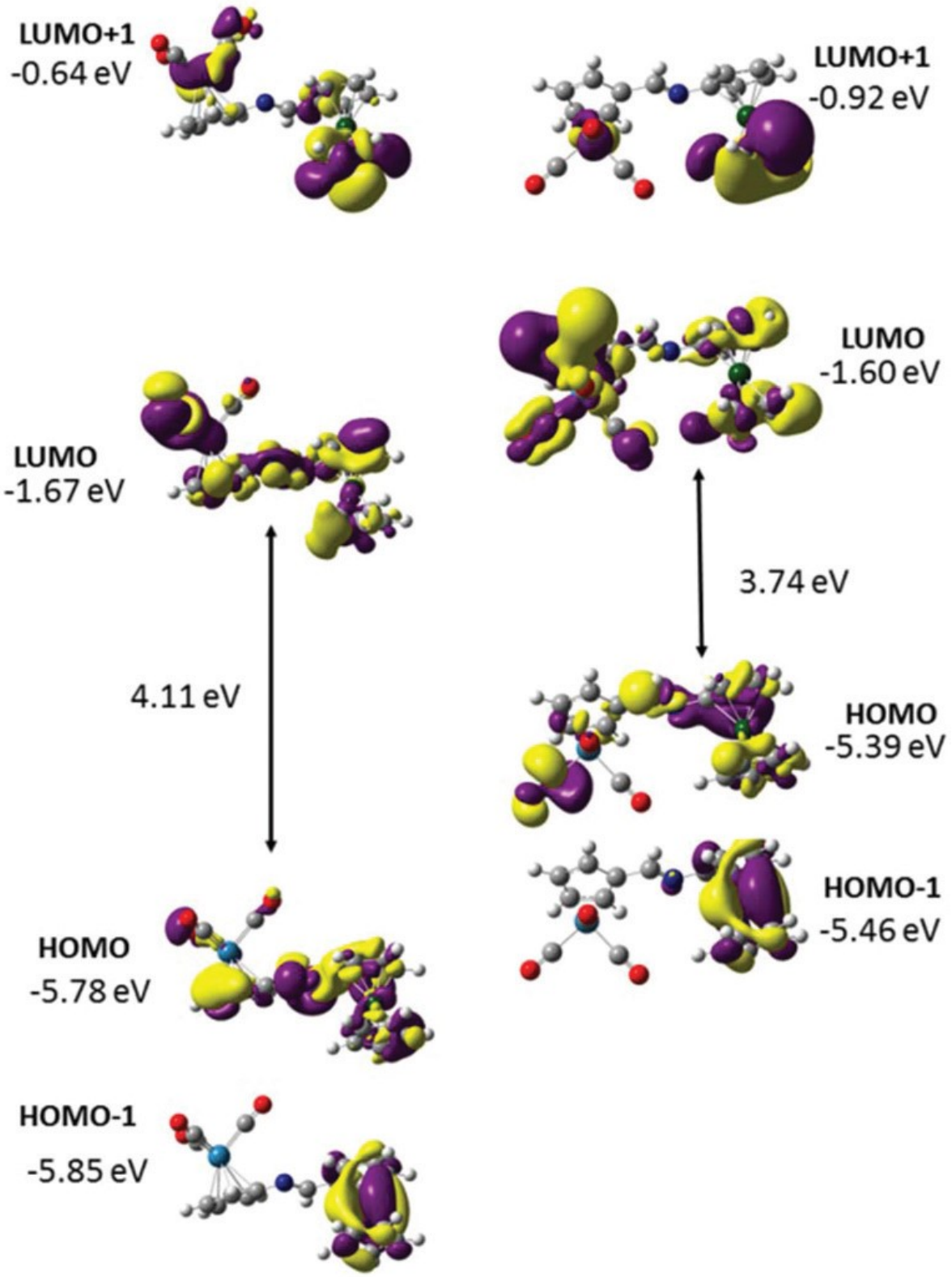

899

900

901 **FIGURE 9**

902

903

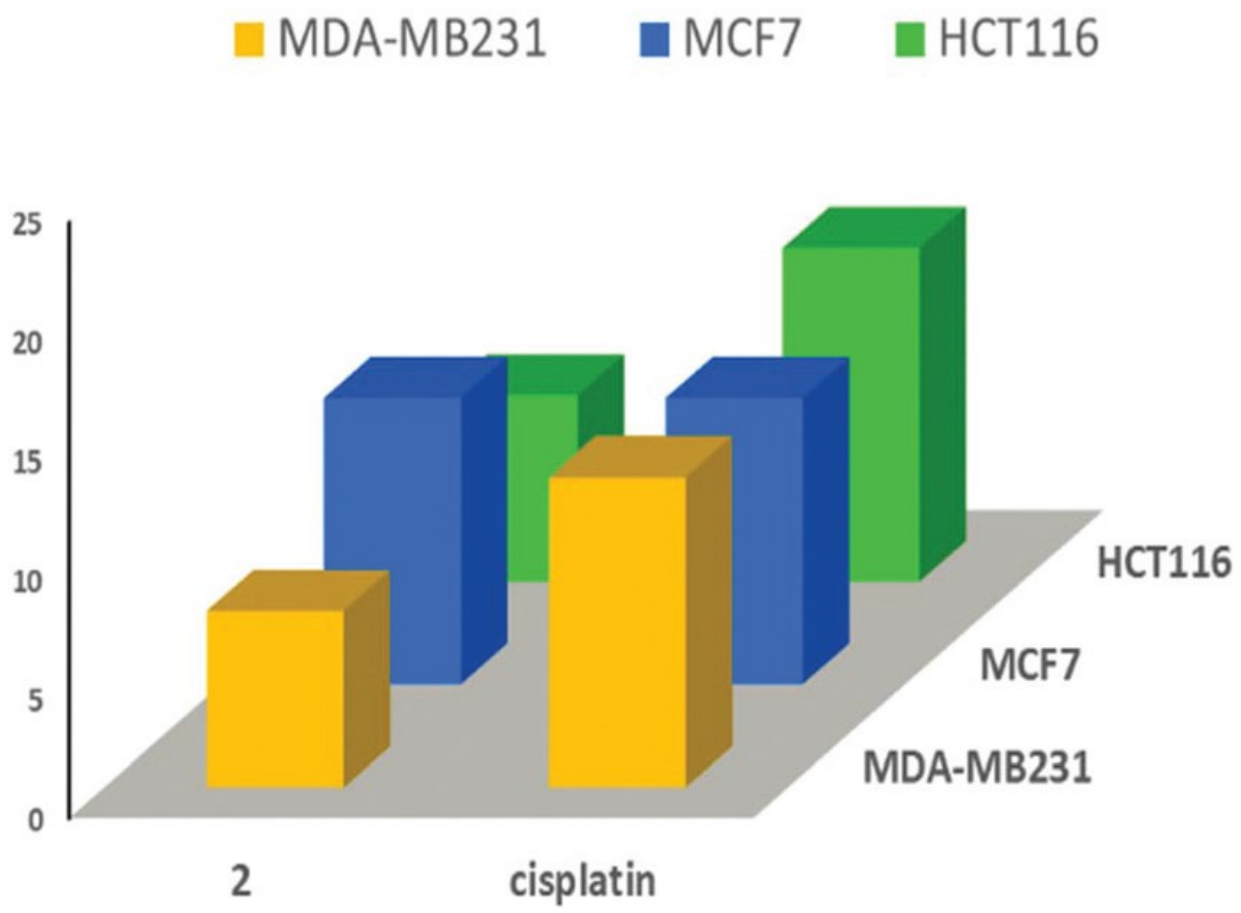

904

905

Table 1 Selected bond lengths (in Å), bond angles (in deg.), and angles between relevant planes (in deg.) of aldimines: [(η5-C5H5)Fe{(η5-C5H4)-CHvN-(η5-C5H4)}Re(CO)3] (1) and [(η5-C5H5)Fe{(η5-C5H4)-NvCH-(η5-C5H4)}Re(CO)3] (2). Standard deviations are given in parenthesis

	1	2
Bond lengths		
N1–C11	1.276(6)	1.276(6)
N1–C12	1.406(7)	—
N1–C10	—	1.430(2)
C10–C11	1.443(7)	—
C11–C12	—	1.463(3)
Re1–C17	1.912(6)	1.9145(19)
Re1–C18	1.916(5)	1.9223(19)
Re1–C19	1.910(5)	1.9170(18)
O1–C17	1.153(7)	1.150(2)
O2–C18	1.150(6)	1.150(2)
O3–C19	1.156(6)	1.148(2)
Fe1–C[a]	2.045(8)	2.046(4)
Re1–C[b]	2.310(19)	2.309(7)
Bond angles		
N1–C11–C[c]	121.6(5)	120.76(17)
C–Re–C[d]	89.6(5)	89.91(3)
Angles between main planes[e]		
I and II	1.3	1.1
II and III	12.6	7.7
II and IV	11.6	5.4
III and IV	11.2	3.10

Table 2 The summary of electrochemical data [anodic (Epa)i, cathodic (Epc)i potentials and the separation between peaks [ΔE = (Epa)I − (Epc)I'] for the new aldimines R1-CHvN-R2 (in V); intensity ratio (Ipa/Ipc). Data were obtained at a scan rate υ = 250 mV s−1 and referenced to the ferrocene/ferricinium couple (Fc/Fc+) (for the identification of the peaks, see Fig. 5)

	R^1	R^2	E^{I}_{pa}	E^{I}_{pc}	ΔE	I_{pa}/I_{pc}	$E_{1/2}$	E^{II}_{pa}	E^{II}_{pc}	E^{III}_{pc}
1	Ferrocenyl	Cyrhetrenyl	0.208	0.135	0.073	1.02	0.172	1.297	0.294	—
2	Cyrhetrenyl	Ferrocenyl	0.057	−0.008	0.065	1.04	0.025	1.420	0.260	0.306

Table 3 Absorption and emission spectroscopic data for aldimines R1-CHvN-R2 (1 and 2) in CH2Cl2 at 298 K. Wavelengths, λi (in nm), logarithms of the extinction coefficients {logε, in parenthesis (ε in M−1 cm−1)}, and excitation and emission wavelengths [λexc. and λem., respectively]

Aldimines R^1-CH=N-R^2			Absorption spectroscopic data				Emission spectroscopic data			
	R^1	R^2	λ_1	λ_2	λ_3	λ_4	$\lambda_{exc.}$	$\lambda_{em.}$		
1	Ferrocenyl	Cyrhetrenyl	473(3.2)	[a]	234(4.4)	220(4.1)	477 385	551 406	432	457
2	Cyrhetrenyl	Ferrocenyl	475(3.3)	383(3.4)	314(4.1)	230(4.3)	473 385	549 405	431	456

[a] Shoulder at ≈380 nm (see text).

Table 4 Relative free energies (ΔG) of isomers, 1b, 2a and 2b in relation to the value obtained for the most stable isomer (1a) in vacuum and in CH2Cl2

	ΔG_r (in kcal mol^{-1})		
	1b	**2a**	**2b**
In vacuum	1.58	1.32	0.64
In CH_2Cl_2	3.26	2.26	1.94

931 **Table 5** Cytotoxic activities of the new aldimines (1 and 2) and cisplatin (IC50 values in μM) against
932 the MCF7 (breast), triple negative MDA-MB231 (breast) and HCT-116 (colon) cell lines together with
933 the values obtained in the human skin fibroblast BJ cell line. For comparison purposes, values obtained
934 for cisplatin under identical experimental conditions are also given

935

	IC_{50} values[a]		
	1	2	Cisplatin
MCF7	>30	12 ± 5.2	12 ± 2.8
MDA-MB231	>30	7.4 ± 1.5	13 ± 1.8
HCT-116	>30	7.8 ± 3.3	14 ± 1.0
BJ	71 ± 2	21 ± 2	23 ± 2

[a] Data are shown as the mean values of two experiments performed in triplicate with the corresponding standard deviations.

936

937

Table 6 Crystal data and details of the refinement of the crystal structures of the new aldimines: [(η5-C5H5)Fe{(η5-C5H4)-CHvN-(η5-C5H4)}Re (CO)3] (1) and [(η5-C5H5)Fe{(η5-C5H4)-NvCH-(η5-C5H4)Re(CO)3] (2)

	1	2
Empirical formula	$C_{19}H_{14}FeNO_3Re$	$C_{19}H_{14}FeNO_3Re$
Formula weight	546.36	546.36
T/K	100(2)	100(2)
Crystal sizes/mm × mm × mm	0.120 × 0.087 × 0.047	0.208 × 0.091 × 0.051
λ/Å	0.71073	0.71073
Crystal system	Orthorhombic	Triclinic
Space group	*Pbca*	$P\bar{1}$
a/Å	20.2799(7)	7.7538(3)
b/Å	7.3753(3)	10.0032(3)
c/Å	22.2740(9)	11.4058 (4)
α/°	90	99.296(2)
β/°	90	104.9040(10)
γ/°	90	98.3590(10)
V/Å^3	3331.5(2)	827.32(5)
Z	8	2
D_{calc}/mg mm^{-3}	2.3179	2.193
μ/mm^{-1}	8.149	8.203
F(000)	2080	520
2θ range for data collected/°	From 2.008 to 28.303	From 2.158 to 30.570
Index ranges	$-26 \leq h \leq 27$ $-8 \leq k \leq 9$ $-25 \leq l \leq 29$	$-11 \leq h \leq 11$ $-14 \leq k \leq 14$ $-16 \leq l \leq 16$
N. of reflections (collected)	21 377	37 637
N. of independent reflections, R_{int}	4125, R_{int} = 0.0594	5064, R_{int} = 0.0306
N. of data	4125	5064
N. of parameters	226	226
Goodness of fit on F^2	1.027	1.112
Final R indices [$I > 2\sigma(I)$]	R_1 = 0.0336, wR_2 = 0.0582	R_1 = 0.0150, wR_2 = 0.0311
Final R indices (all data)	R_1 = 0.0587, wR_2 = 0.0601	R_1 = 0.0179, wR_2 = 0.0317
Largest diff. peak and hole/eÅ^{-3}	0.888 and −1.093	0.691 and −1.031